Nanoscale

REVIEW

Shape matters: synthesis and biomedical applications of high aspect ratio magnetic nanomaterials

Cite this: DOI: 10.1039/c5nr01100k

Raluca M. Fratila,*[a,b] Sara Rivera-Fernández[a] and Jesús M. de la Fuente*[a,c,d]

High aspect ratio magnetic nanomaterials possess anisotropic properties that make them attractive for biological applications. Their elongated shape enables multivalent interactions with receptors through the introduction of multiple targeting units on their surface, thus enhancing cell internalization. Moreover, due to their magnetic anisotropy, high aspect ratio nanomaterials can outperform their spherical analogues as contrast agents for magnetic resonance imaging (MRI) applications. In this review, we first describe the two main synthetic routes for the preparation of anisotropic magnetic nanomaterials: (i) direct synthesis (in which the anisotropic growth is directed by tuning the reaction conditions or by using templates) and (ii) assembly methods (in which the high aspect ratio is achieved by assembly from individual building blocks). We then provide an overview of the biomedical applications of anisotropic magnetic nanomaterials: magnetic separation and detection, targeted delivery and magnetic resonance imaging.

Received 15th February 2015,
Accepted 1st April 2015

DOI: 10.1039/c5nr01100k

www.rsc.org/nanoscale

[a]*Instituto de Nanociencia de Aragon (INA), Universidad de Zaragoza, C/Mariano Esquillor s/n, 50018 Zaragoza, Spain. E-mail: rmfratila@gmail.com, rfratila@unizar.es, jmfuente@unizar.es*
[b]*Fundación ARAID, C/María de Luna 11, Edificio CEEI Aragón, 50018 Zaragoza, Spain*
[c]*ICMA-CSIC, C/Pedro Cerbuna 12, 50009 Zaragoza, Spain*
[d]*Institute of Nano Biomedicine and Engineering, Key Laboratory for Thin Film and Microfabrication Technology of the Ministry of Education, Research Institute of Translation Medicine, Shanghai Jiao Tong University, Dongchuan Road 800, 200240 Shanghai, People's Republic of China*

1. Introduction

Nanomaterials possess unique physicochemical properties that differ considerably from those of the corresponding bulk material. These novel chemical, optical, electronic or magnetic properties have been applied in different fields, ranging from optoelectronics and magnetic devices to catalysis and biomedicine. Taking into account the fact that the sizes of most biologically relevant molecules and structures fall within the

Dr Raluca M. Fratila

Dr Raluca M. Fratila obtained her PhD in Chemistry from University Politehnica Bucharest (Romania) in 2005. She accomplished postdoctoral stays at the University of Basque Country, San Sebastian, Spain (2006–2008), and the University of Twente, Enschede, The Netherlands (2009–2013). Since November 2013, she is an ARAID-EU researcher at the Institute of Nanoscience of Aragón (INA), University of Zaragoza, Spain. Her research interests include bioorganic and bioorthogonal chemistry, microfluidics, NMR spectroscopy, magnetic resonance imaging (MRI) and magnetic nanoparticles for biomedical applications.

Sara Rivera-Fernández

Sara Rivera-Fernández studied Chemistry at U.N.E.D. (Spain, 2007) and obtained her MSc from the University of Zaragoza (2010, under the supervision of Prof. Pedro Merino). Currently, she works at the Institute of Nanoscience of Aragon (University of Zaragoza) in the group of Dr Jesús M. de la Fuente. Her research focuses on the synthesis, functionalization and characterization of magnetic nanoparticles for biomedical applications.

nanoscale dimension, it comes as no surprise that interfacing nanomaterials with biology and medicine have led to some of the most promising applications of nanotechnology in the past two decades.

Historically, research on nanomaterials for biomedical applications has focused on spherical nanomaterials (*e.g.* gold nanoparticles, quantum dots and magnetic nanoparticles). More recently, high aspect ratio nanomaterials such as nanowires, nanorods, nanotubes or linear assemblies of nanoparticles (nanochains) have begun to receive attention because of their elongated geometry, which translates into magnetic, optical, electrical or chemical anisotropy. As a consequence of their anisotropic properties, high aspect ratio nanomaterials are likely to interact with biological entities in completely different ways than their spherical counterparts. For instance, some high aspect ratio nanomaterials (carbon nanotubes[1,2] and filament-shaped polymer micelles[3]) have been reported to have a considerably longer blood half-life than spherical nanoparticles, which was attributed to the slower uptake of such nanostructures by macrophages. This has important consequences for biomedical applications because a long circulation time in the bloodstream is a key requirement for *in vivo* targeting, imaging and delivery using nanomaterials.[1–6] Moreover, shape anisotropy offers new possibilities for functionalization towards bioapplications. On the one hand, the large surface area of these nanostructures offers the possibility of multivalent interactions between targeting ligands and receptors, thus facilitating cell internalization.[4,5,7] On the other hand, heterostructured multi-segment nanowires can be selectively functionalized with different biomolecules to enhance their biocompatibility or targeting ability.[8]

This review describes recent advances in the field of *magnetic high aspect ratio nanomaterials*. We chose to focus only on magnetic nanomaterials based on the fact that spherical magnetic nanoparticles have shown the most promising bioapplications so far when compared to other nanostructured materials, for example in magnetic hyperthermia therapy of cancer, targeted drug delivery, tissue engineering, bioseparations and biosensing, as well as in the field of contrast agents for magnetic resonance imaging.[9–16] Therefore, we expect a similar interest in growth regarding anisotropic magnetic nanomaterials. In addition to the above-mentioned general features of high aspect ratio nanomaterials (longer blood circulation time and the possibility of multivalent and/or selective biofunctionalization), magnetic anisotropy is attractive for magnetic resonance imaging (MRI) applications, as well as for magnetic separation and manipulation. Due to linear clustering, some high aspect ratio magnetic nanomaterials showed increased transverse relaxivity when compared to their spherical counterparts.[4,17,18] Anisotropic magnetic nanomaterials have higher magnetic moments than spherical ones and therefore can be manipulated using weaker magnetic fields, opening up new possibilities for magnetic targeted delivery and therapy, as well as for magnetic cell separation.[8] The review is organised as follows. We start by presenting the main classes of high aspect ratio magnetic nanomaterials to be discussed in this work and the synthetic methods that allow for their fabrication. To facilitate the reading, we include for each nanomaterial, immediately after describing its synthesis, a brief discussion of its magnetic properties and how these are influenced by anisotropy. We then give an overview of the applications of high aspect ratio nanomaterials in biomedicine. We wrap up the discussion with a brief summary and a critical perspective of the field.

2. Synthesis and magnetic properties of high aspect ratio magnetic nanomaterials

During the last decade, the nanotechnology nomenclature has been enriched with terms such as “nanotubes”, “nanowires”, “nanochains”, “nanoworms”, “nanobars”, “nanorods” and “nanoneedles”, to name but a few. These names are generally related to the shape of nanomaterials rather than to their actual aspect ratio and chemical structure and, to date, there is no universal nomenclature accepted for non-spherical nanomaterials.[19] The aspect ratio is determined by dividing the major axis of a shape by the width of its minor axis. Hence, a sphere has an aspect ratio of 1. Although some authors consider that nanowires have a higher aspect ratio than nanorods,[20] there is no strict differentiation between these two nanostructures.[21] In this review we will employ the nomenclature reported by different authors and we will discuss three main geometries of high aspect ratio magnetic nanomaterials: nanowires/nanorods, nanotubes and chain- or worm-like assemblies (Fig. 1; see Table 1 for a summary of the types of high aspect ratio nanomaterials that form the subject of this discussion).

Dr Jesus M. de la Fuente

Dr Jesus M. de la Fuente obtained his PhD in 2003 (University of Seville, Spain). In 2007 he obtained a permanent ARAID position at the Institute of Nanoscience of Aragón (University of Zaragoza), where he established his own research group. His main research interests include the development of general and simple strategies for the biofunctionalization of nanoparticles and surfaces. Dr de la Fuente is the recipient of an ERC Starting Grant (Nanopuzzle) and he has co-authored more than 115 publications (H index of 31). Currently, Dr de la Fuente is affiliated to the Institute of Materials Science of Aragón (CSIC-UNIZAR).

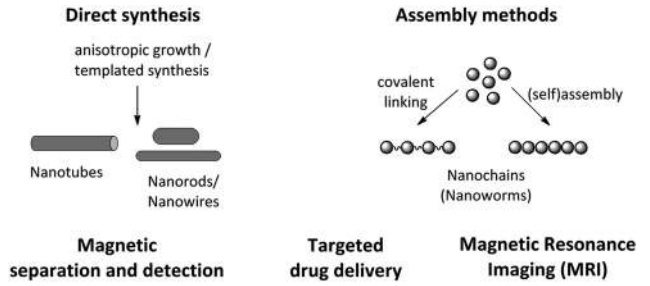

Fig. 1 High aspect ratio nanomaterials discussed in this work and their biomedical applications.

It is rather difficult to classify the synthetic approaches used to obtain high aspect ratio magnetic nanomaterials, as many different methodologies have been addressed. Generally, they can be divided into two main classes: *direct synthesis* (the morphology is controlled during the synthesis by tuning the synthetic conditions or by using appropriate templates) and *assembly methods* (the high aspect ratio nanomaterial is assembled from individual building blocks, either during the synthesis or in a post-synthetic step). However, some examples of hybrid synthetic methods involving the use of nucleic acids or carbon nanotube templates together with spherical magnetic nanoparticles can be found in the literature. For the sake of uniformity, we will discuss these more exotic approaches (ref. 58,60–64) at the end of section 2.1.2, together with classical template-assisted synthesis. In general, direct synthesis leads to tube-, rod- and wire-like magnetic nanomaterials, while nanostructures such as nanochains and nanoworms are obtained by assembly methods. An overview of these synthetic methods is given as follows, discussing their advantages and drawbacks. Many articles report only the synthesis of high aspect ratio nanomaterials, without further exploring their bioapplications. Therefore, we will highlight some synthetic procedures that yielded high aspect ratio nanostructures with potential bioapplications, but our focus will be on the synthesis of high aspect ratio nanomaterials that have already been tested for biomedical applications. Whenever possible, we will provide insights into the mechanisms proposed for the formation of different types of anisotropic nanostructures.

2.1 Direct synthesis

2.1.1 Chemical synthesis. The aspect ratio of nanomaterials can be tailored by fine-tuning synthetic parameters such as reaction media, ratio and concentration of precursors and/or reagents, reaction time, temperature and so forth. Importantly, the surface chemistry of the nanomaterial, which is fundamental for future biomedical applications (see section 3) can be also controlled during the synthesis. In this section, we discuss relevant literature examples reporting on strategies to promote the growth of the anisotropic magnetic nanomaterials of different morphologies and aspect ratios. These strategies involve different chemical methods, from co-precipitation to thermal decomposition of precursors, microemulsion and hydrothermal growth. Although it seems generally accepted that the crystallization process governs the growth of 1D nanostructures, the exact mechanisms of formation of such nanostructures are often not fully understood. In this section, we will present and discuss the mechanisms reported in the literature; for further details of strategies to control the growth of high aspect ratio nanomaterials (although not focused on magnetic anisotropic nanomaterials), we direct interested readers to the review of Xia *et al.*[22]

Table 1 Types of high aspect ratio magnetic nanomaterials[a]

Type of nanomaterial	Chemical composition	Synthetic method	Aspect ratio	Magnetic properties	Ref.
Nanotubes, nanorods	IO	Hydrothermal	2,7	Ferromagnetic	23,24
Nanorods	IO	Microwave-assisted reduction	3	Ferromagnetic	25
Nanorods	IO	Co-precipitation	2	Superparamagnetic	27
Nanorods, nanowhiskers	IO	Thermal decomposition	5; 10; 4	(Super)paramagnetic/ ferromagnetic	30,31,33
Nanowires	IO	Microemulsion	>100	Superparamagnetic/ ferromagnetic	32
Nanowires	IO	Ultrafiltration	Tuneable (4–10)	—	35
Nanorods nanowires	Ni, Au–Ni, IO	Porous membranes-templated	Tuneable	—	40–52
Nanotubes, nanowires	IO, Co IO, Au–(Co) IO	Carbon nanotube/ DNA-templated	—	Superparamagnetic	54–65
Nanochains, nanowires, nanorods	IO, $FeNi_3$	Magnetic assembly	Tuneable (4–20)	Superparamagnetic/ ferromagnetic	67–70,73–79,81,82
Nanoworms, nanochains	IO, Co IO	Polymer assembly, self-assembly	—	Superparamagnetic	4,5,88
Nanochains	IO	Covalent linking	3–5	Superparamagnetic	89,91

[a] IO: Iron oxide (α-Fe_2O_3: hematite; γ-Fe_2O_3: maghemite; Fe_3O_4: magnetite).

Wu *et al.* reported a systematic study of the effect of several parameters (concentrations of ferric ions and additives, reaction time) on the size and morphology of iron oxide nanoparticles obtained by the hydrothermal treatment of $FeCl_3$ in the presence of sulphate and phosphate additives.[23] By tuning the reaction times and the concentration of ferric chloride, the authors were able to control the shape of hematite (α-Fe_2O_3) nanoparticles, as shown in Fig. 2a. Short magnetite nanotubes (SNT) with an aspect ratio of 2 (see Fig. 2b for representative SEM and TEM images) were obtained at long reaction times (6–12 h) and a concentration of $FeCl_3$ of 0.04 M. Moreover, the geometry of the resulting nanostructures was also affected by the type and ratio of the additives used (Fig. 2c), with phosphate ions playing a crucial role in inducing shape anisotropy. This observation is in line with a previous literature report by Brown and co-workers, who attributed the formation of α-Fe_2O_3 nanorods to the preferential adsorption of the phosphate surfactant to the *c*-axis of α-Fe_2O_3, which promoted the growth of rod-like structures.[24] Importantly, the hematite SNTs synthesised by Wu *et al.* could be transformed into the corresponding magnetite (Fe_3O_4) and maghemite (γ-Fe_2O_3) nanostructures by annealing under a reducing atmosphere with retention of their size and morphology. In terms of magnetic properties, both magnetite and maghemite nanotubes showed a ferromagnetic behaviour, with a higher saturation magnetization (M_s) value for the Fe_3O_4 ones. Although no applications are reported in this study, the authors note that both types of short nanotubes could have potential for bioseparations because of their good magnetic response. The nanotubes could be quickly separated in the presence of a magnet and easily re-dispersed by simple shaking.

Microwave-assisted synthesis of nanomaterials is becoming increasingly popular, following a similar trend in organic chemistry. Motte and co-workers synthesized magnetic nanorods by a two-step one-pot procedure involving the microwave reduction of precursor nanorods obtained in the first step.[25] In this case, the shape control is achieved during the synthesis of the precursor (akaganeite β-FeOOH) using dopamine, which is known for its strong affinity for Fe(III). In the absence of dopamine ligands, mainly hexagonal nanoparticles were

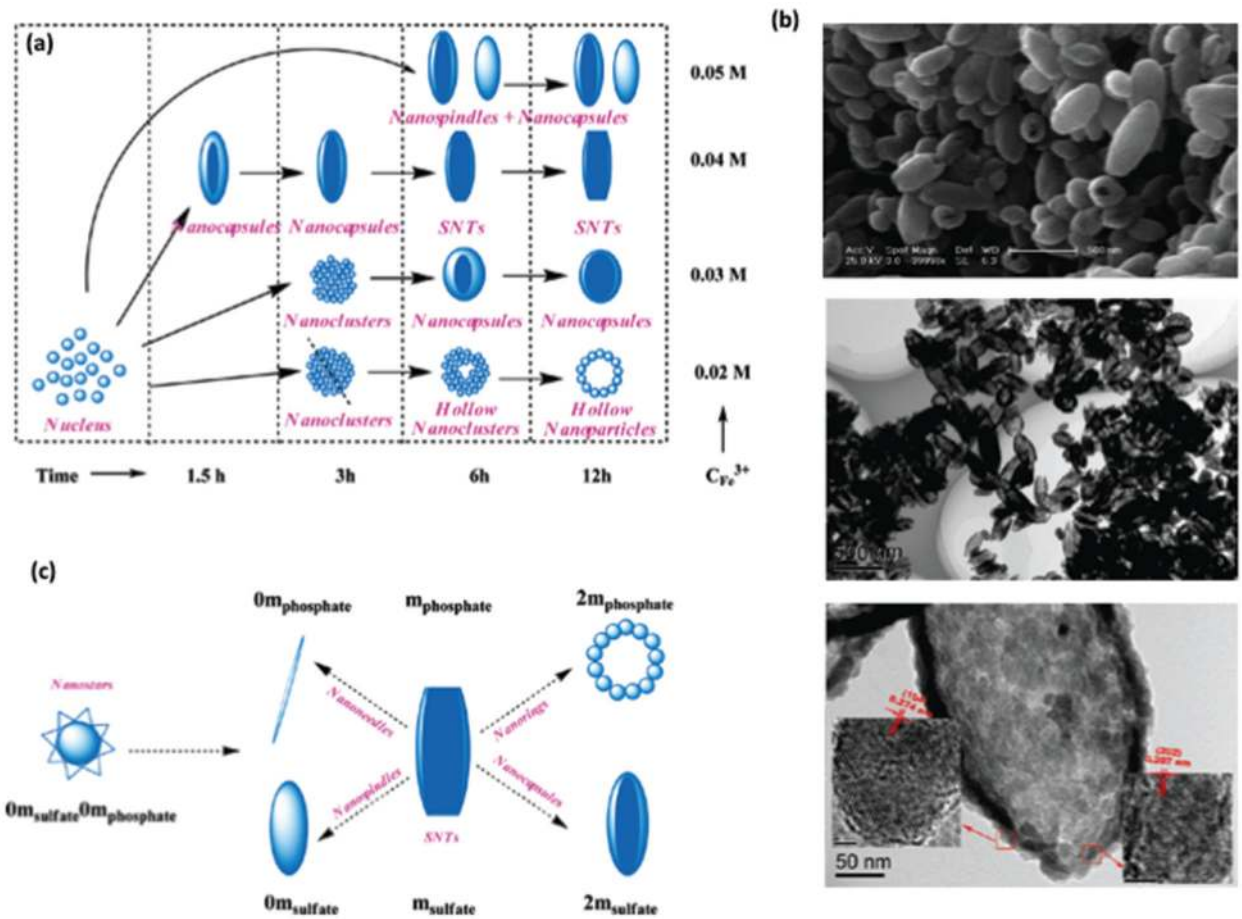

Fig. 2 Anion-controlled synthesis of short magnetic nanotubes. (a) Shape evolution of hematite nanostructures with time and ferric ions concentration. (b) Top and centre: SEM and low magnification TEM images of nanotubes. Bottom: high-resolution TEM (HRTEM) image of a single hematite nanotube. Scale bar of the inset in the HRTEM picture is 2 nm. (c) Formation process of hematite structures mediated by phosphate and sulphate anions. Reprinted with permission from ref. 23. Copyright 2010, American Chemical Society.

obtained, while its presence promoted the growth of rod-shaped nanoparticles whose aspect ratio was inversely proportional to the reaction times, decreasing from 5.8 after 2 h reaction time to 4.6 after 4 h. Dopamine plays here a similar role to that of phosphate ions in the above-discussed examples,[23,24] favouring the growth of rod-like structures along the *c*-axis of the β-FeOOH crystal. In the second step, microwave irradiation at 100 °C and 200 W promoted the reduction of β-FeOOH to Fe_3O_4/γ-Fe_2O_3 nanorods, as shown by XRD analysis. Interestingly, the geometry of the final particles strongly depended on the reaction conditions. After four microwave cycles the rod-like geometry was attained, although the aspect ratio decreased from 5.8 to 3.2, suggesting that the reduction took place through a dissolution–recrystallization mechanism. However, six or eight microwave cycles resulted in a shape change from rods to hexagonal nanoparticles. Tartaj and co-workers reported a similar approach for controlling the morphology in the first step of the synthetic process.[26] Their simple procedure for the synthesis of nanorods and nanorices with tuneable surface chemistry consisted in preparing rod- and rice-like goethite nanoparticles by aerobic oxidation of $FeSO_4$ and coating them with an inorganic alumina or zirconia layer. Finally, to promote the formation of superparamagnetic iron oxide spinels, the nanorods were heated under a H_2 atmosphere. The choice of the coating layer was motivated by the potential biological applications of these nanostructures. The fact that alumina is positively charged at physiological pH could favour their cellular uptake by negatively charged membranes, while zirconia could be functionalized with phosphate moieties for improved stability and functionality.

Nath *et al.* developed a simple, high-yield and scalable water-based synthesis of dextran-coated iron oxide (DION) superparamagnetic nanorods.[27] The protocol involves a typical co-precipitation of Fe(II) and Fe(III) salts in the presence of a base (ammonium hydroxide). Interestingly, the addition of the polymer 30 s after the beginning of the nucleation process favoured the formation of monodisperse rod-shaped magnetite nanocrystals (aspect ratio of 2.3), whereas when the dextran was present in the reaction medium from the beginning of the synthesis, poorly crystalline spherical nanoparticles were obtained. Although no detailed growth mechanism was presented, the purity and size distribution of the polymer seemed to play a key role in controlling the morphology of the nanoparticles. High purity dextran with a narrow size distribution was assumed to bind to the surface of iron oxide nanocrystals, directing the preferential growth of nanorods, whilst less pure dextran polymers displaying two main populations seemed to interfere with the directional growth process and yielded polydisperse spherical iron oxide nanoparticles. The superparamagnetic behaviour of the nanorods was attributed to the presence of magnetite in their structure, which was confirmed by both X-ray diffraction data and X-ray photoelectron spectroscopy (XPS). Importantly, the DION rods synthesised by adding dextran at 30 and 60 s from the beginning of the reaction showed high transverse relaxivities ($R_2 \approx 300$ mM^{-1} s^{-1}), which makes them promising candidates for magnetic resonance imaging and sensing applications.

Thermal decomposition of Fe(III) organic complexes (iron oleate and iron acetylacetonate) in the presence of oleic acid and oleylamine is usually the method of choice for the synthesis of spherical iron oxide nanoparticles because it produces nanoparticles with excellent crystallinity and very narrow size distribution.[28,29] However, to date, there have been only scarce reports on the use of this methodology for the synthesis of anisotropic iron oxide nanomaterials. This could be related to an insufficient understanding of the growth mechanism, including the role of reaction parameters such as temperature and ligands. Starting from iron oleate and sodium oleate as precursors, Bao *et al.* were able to tune the aspect ratio of γ-Fe_2O_3 nanorods by controlling the reaction temperature, observing that the higher the temperature, the lower the aspect ratio of the obtained rods.[30] The authors also reported the effect of the precursors on the morphology of the resulting nanoparticles as replacement of sodium oleate by oleic acid resulted in only spherical nanocrystals. Palchoudhury *et al.* reported recently the first synthesis of ultrathin elongated iron oxide nanostructures called "nanowhiskers" by thermal decomposition of Fe(III) oleate (Fig. 3a).[31] The authors conducted a comprehensive mechanistic study to account for the role of the ligands in the growth process. Density functional theory (DFT) calculations (Fig. 3b) revealed that the Fe(III) oleate complex has a quasi-octahedral structure with two of the three oleate ligands having much lower binding energies (7.0 and 10.5 eV) than the third one (39.2 eV). Thermogravimetric analysis (TGA) experiments provided further confirmation of this difference in the ligand coordination environment, with two regions which could be clearly attributed to the loss of the two weakly bound ligands between 150 and 230 °C (Fig. 3c, region a) and to the decomposition of the third ligand at 230–295 °C (Fig. 3c, region b). In light of these results, the authors postulated that the third oleate ligand plays a critical role in directing the growth of the nanowhiskers. Their hypothesis was supported by the fact that thermal decomposition using Fe(II) oleate (which has two ligands with similar binding energies) as the precursor instead of Fe(III) oleate yielded only irregularly shaped, aggregated nanoparticles. Furthermore, experiments performed using surfactants that have a weaker, respectively a stronger binding to iron oxide nanoparticles than oleic acid (trioctylphosphine oxide (TOPO) and oleylamine (ON), respectively) produced nanostructures with similar whisker shapes. These nanowhiskers did not contain any traces of TOPO or oleylamine on their surface, as indicated by their infrared spectra, further confirming that the third oleate ligand directs the formation of such high aspect ratio nanostructures.

Yang and co-workers demonstrated the effect of annealing temperature on the morphology and chemical structure of magnetic nanowires.[32] Iron(II) oxalate dihydrate nanowires with a diameter of 100 nm and lengths of several tens of micrometres were firstly synthesized by microemulsion and subsequently annealed at different temperatures and under

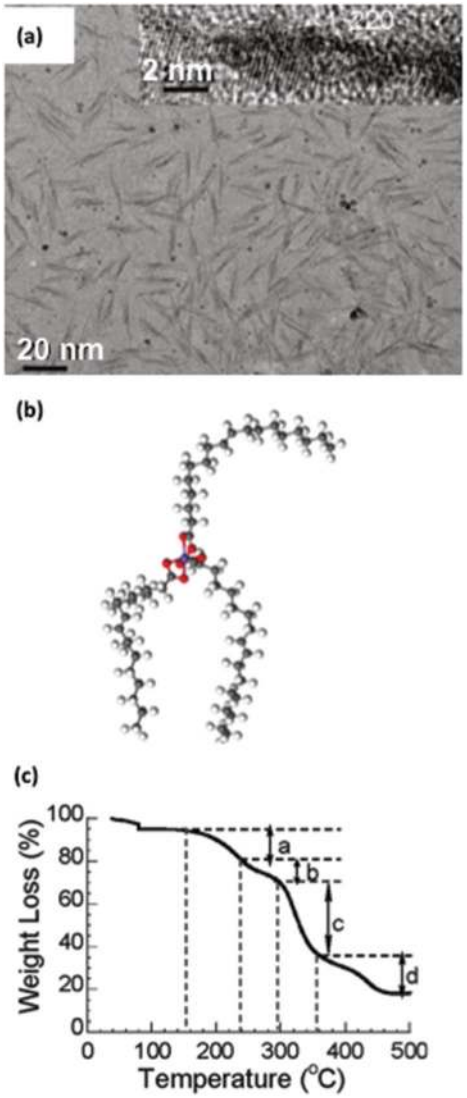

Fig. 3 (a) TEM image of iron oxide nanowhiskers and HRTEM inset. (b) Optimised structure of the Fe(III) oleate complex. (c) TGA plot revealing the thermal decomposition behaviour of the iron oleate complex. Reprinted with permission from ref. 31. Copyright 2011, American Chemical Society.

different atmospheres. In air at 550 and 700 °C, respectively, porous α-Fe_2O_3 nanowires maintaining the morphology of the $FeC_2O_4{\cdot}H_2O$ precursor were obtained. However, when the annealing was performed at 400 °C under an Ar/H_2 atmosphere, Fe_3O_4 nanowires were obtained, as indicated by TEM and infrared spectroscopy. Yet another example of how the reaction temperature can control the shape, structure and magnetic properties of magnetic nanomaterials was reported by Zhang *et al.* for the thermal decomposition of $Fe(acac)_3$.[33] When the reaction was carried out in water at 140 °C for 12 h in a sealed autoclave, uniformly sized superparamagnetic hematite nanorods were obtained. However, increasing the temperature to 180 °C led to different morphologies of hematite nanostructures, depending on the reaction time: mixtures of nanorods and spherical nanoparticles after 3 h and nanocubes after 8 h. On the other hand, direct thermolysis of the $Fe(acac)_3$ precursor in air at 300 °C for 3 h resulted in quadrate maghemite nanocrystals displaying a ferromagnetic behaviour.

Ionic liquids (ILs) can be successfully used as solvents for the thermal decomposition of $Fe(CO)_5$ to regulate the shape and chemical composition of the obtained iron oxide nanoparticles, as reported by Lee and co-workers.[34] Interestingly, when ionic liquids alone were used as the reaction medium, only maghemite nanobars were obtained. When the synthesis was carried out in mixtures of IL and dimethylformamide (DMF) at ratios of 1 : 1.5 and 1 : 3, the formation of magnetite anisotropic nanoparticles (nanobars, respectively nanowires) was observed by TEM. Moreover, the ILs also acted as surface stabilizers, eliminating the need for additional surfactants typically employed in thermal decompositions. The examination of the magnetic properties of the maghemite nanobars by superconducting quantum interference device (SQUID) magnetometry revealed that they were superparamagnetic; moreover, they showed potential for use as contrast agents for MRI. However, the authors did not conduct a comparative study on the magnetic behaviour of the corresponding magnetite high aspect ratio nanoparticles.

In a rather original approach, Chang *et al.* employed ultrafiltration for the synthesis of γ-Fe_2O_3 nanowires coated with a biocompatible polymer (chitosan) in a simple, one-step, room temperature co-precipitation of Fe(II) and Fe(III) salts.[35] In this case, the tangential force is driving the formation of elongated nanoparticles, while the concentration of the NaOH solution plays a key role in controlling their size and shape. At low NaOH concentrations (5% w/w), rod-like particles with an aspect ratio of 4 were formed. A gradual increase in the concentration of NaOH resulted in the formation of nanowires with aspect ratios higher than 10.

2.1.2 Template-assisted synthesis. This synthetic approach makes use of premade nanoporous templates (hard templates) or biomolecules (soft templates) to control the morphology and aspect ratio of nanomaterials. Hard templates usually consist of rigid materials (zeolites, alumina, and block copolymer films) containing pores or channels and have the advantage of a good control over the size and dispersity of the final nanomaterials. Nevertheless, their synthesis can be time-consuming and expensive. Soft templates such as biological macromolecules and pre-ordered polymeric structures can act as templates only (meaning that they are removed after synthesis to afford the stand-alone inorganic magnetic nanomaterial). However, their chemical properties can be advantageously used for tuning the solubility, biocompatibility and surface functionality of the resulting hybrid organic–inorganic nanoconstructs. For comprehensive reviews on template-directed synthesis of different classes of magnetic, but also non-magnetic nanomaterials, interested readers can refer to several literature reviews.[36–39]

Electrodeposition of metallic salts inside alumina or polycarbonate porous membranes is one of the most popular methods to grow both single-segment and multi-segment

nanowires in hard templates. Electrochemical deposition is fast, relatively easy to perform and does not require expensive instrumentation or high pressure and temperature conditions. Typically, in the first step of the process a thin film of metal is deposited on one face of the template to serve as a working electrode. A sacrificial metal layer can be introduced before the deposition step in order to avoid deformations at one end of the rods or wires. Then, the deposition of the desired material(s) is performed and in the final steps the working electrode, sacrificial layer and template are dissolved to release the high aspect ratio nanostructures (Fig. 4).

Several authors applied this method for the synthesis of magnetic nickel nanowires[40–42] and multifunctional magnetic gold–nickel nanowires[43–45] in large quantities and with excellent monodispersity. Moreover, by tuning the chemical composition of Ni/Cu nanowires, Reich and co-workers demonstrated that it is possible to tailor their magnetic properties.[46] Nanowires fabricated by electrodeposition into polycarbonate membranes showed different magnetic responses to an external magnetic field depending on the aspect ratio of the Ni and Cu layers. Nanowires containing rod-shaped layers (diameter 100 nm, length 1000 nm, aspect ratio of 10) aligned parallel to the magnetic field, while nanowires with disc-shaped layers (diameter 100 nm, length 10 nm, aspect ratio of 0.1) aligned perpendicular to the applied field. Pondman *et al.* synthesised short (2.6 ± 0.3 μm, 150 nm diameter) superparamagnetic Ni nanowires by electrodeposition inside polycarbonate membranes.[47] After dissolution of the membrane, the nanowires were further coated with a gold layer to increase their biocompatibility.

Another methodology to construct high aspect ratio nanomaterials using hard templates consists in the vacuum-assisted infiltration of the components in the pores of the template. McCarthy *et al.* synthesised multimodal (magnetic and fluorescent) nanowires by infiltrating a THF solution of polystyrene, fluorescent coumarin-153 dye and spherical oleic acid-coated 12 nm magnetite nanoparticles into 200 nm porous alumina membranes.[48] The free nanowires were obtained after dissolving the membrane with NaOH, as in the case of electrodeposition methods. The initial spherical magnetite nanoparticles showed a typical superparamagnetic behaviour, with an M_s value of 48.5 emu g^{-1} comparable to previous reports on NPs synthesised in a similar fashion, as observed from vibrating sample magnetometry (VSM) experiments.[49] Unfortunately, the magnetic characterization of the nanowires by VSM was impossible due to practical difficulties related to the geometry of the material. Although the authors conducted a VSM measurement using a polystyrene film loaded with magnetite (with an identical loading to that of the nanowires) and observed a much lower M_s value (5.2 emu g^{-1}) and a small loss of the superparamagnetic behaviour, it is not clear to what extent these data are relevant for the magnetic behaviour of the nanowires. Prina-Mello and co-workers used the same vacuum-assisted infiltration procedure for the preparation of silica nanowires (lengths of 8 ± 2 μm, diameters of 176 ± 50 nm) loaded with magnetite nanoparticles.[50] The authors compared the magnetic properties of the silica nanowires with those of their spherical counterparts, silica-coated magnetite nanoparticles (144 ± 15 nm). The spherical nanostructures showed higher M_s values and a higher content of magnetite than the nanowires; therefore, the benefits of shape anisotropy were not evident in terms of magnetic behaviour. However, the nanowires showed a clear advantage over spherical nanoparticles in terms of surface functionalization with antibodies, aggregation behaviour and flow cytometry applications (see section 3).

Magnetic nanotubes consisting of silica nanotubes coated with Fe_3O_4 nanoparticles on their inner surface were prepared by Lee and co-workers by a "surface sol–gel" method using porous alumina templates of different diameters (60 and 200 nm).[51] The iron oxide nanoparticles present inside the nanotubes were clearly visible on TEM images. Their presence was further confirmed by the superparamagnetic behaviour of the nanotubes, deducted from their room-temperature magnetization curves measured in a superconducting quantum interference device (SQUID). The saturation magnetization values obtained for the 60 and 200 nm nanotubes (2.7 and 2.9 emu g^{-1}, respectively) are in agreement with the values previously reported for magnetite-coated spherical silica nanoparticles (3.2 emu g^{-1}).[52] Interestingly, this method also allows for a differential functionalization of the inner surface of the magnetic nanotubes for biomedical applications (see section 3).

In a different approach, magnetite tubular nanostructures were obtained in a process involving pulsed-laser deposition of Fe_3O_4 onto MgO nanowires, followed by selective etching of the magnesium oxide cores.[53] This simple technique generates single crystalline Fe_3O_4 nanotubes with excellent size homogeneity and controllable dimensions (length, diameter and thickness).

Carbon nanotubes (CNTs) are excellent scaffolds or templates for the construction of anisotropic nanomaterials because of their large surface area. Hybrid CNTs–iron oxide nanomaterials combine the advantages of each individual component and could be promising candidates for different biomedical applications, including MRI, magnetic hyperthermia treatment and drug delivery. Several methods are reported

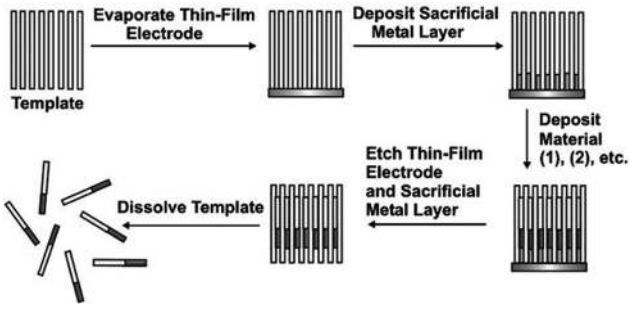

Fig. 4 General scheme describing the fabrication of nanorods/nanowires by electrodeposition into nanoporous templates. Reprinted from ref. 37 with permission from John Wiley & Sons.

to date for the introduction of magnetic nanoparticles on the surface of CNTs. Most of them consist in the *in situ* preparation of the magnetic nanoparticles *via* co-precipitation of Fe(II) and Fe(III) salts or thermal decomposition of precursors in the presence of the CNTs. Yang and co-workers obtained hydrophilic superparamagnetic multiwalled (MW) CNT/Fe_3O_4 hybrids by a classical solvothermal method using diethanolamine to control the growth of the nanoparticles and to prevent their aggregation.[54] However, TEM images recorded at high magnification revealed the presence of nanoclusters composed of several nanocrystals of Fe_3O_4 on the surface of the MWCNTs (Fig. 5a and b). The good water colloidal stability of the hybrids was attributed to the presence of diethylene glycol (used as a solvent) and diethanolamine on the surface of the nanotubes. Alternatively, polymers grafted onto the surface of the CNTs can be used not only to increase the stability of the magnetic nanotubes in water, but also to ensure a more uniform deposition of the Fe_3O_4 nanoparticles and to provide reactive groups for further (multi)functionalization.[55]

Magnetic MWCNT hybrids can also be synthesised by thermal decomposition of ferrocene at 425 °C, resulting in the attachment of iron oxide nanoparticles onto the surface of the nanotubes.[56] In this case, XRD, XPS and Raman spectroscopy experiments revealed that the magnetic material present on the CNTs was mainly Fe_2O_3. The main disadvantage of this method when compared to the solvothermal procedure reported by Yang was that the as-synthesised magnetic nanotubes were not easily dispersible in water, therefore requiring additional polymer coating to render them suitable for biological applications.

Recently, Lamanna *et al.* reported the preparation of MWCNTs decorated with iron oxide nanoparticles (NPs), investigating two different synthetic routes based on ligand exchange or click chemistry, respectively.[57] Ligand exchange between CNTs bearing carboxyl groups and oleic acid-coated NPs (**CNT-IO 1**) resulted in a high loading of nanoparticles on the nanotube surface; moreover, the NPs showed a high tendency to form aggregates (see Fig. 5c). In contrast, click chemistry ligation between azide-functionalized iron oxide NPs and alkyne-modified CNTs allowed for a much better control of the anchoring of NPs onto the surface of the nanotubes and prevented aggregation (**CNT-IO 2**, Fig. 5d). The authors postulated that the different aggregation behaviour observed using the two different strategies was directly related to the number of reactive groups available for functionalization on the surface of the CNTs, being the number of COOH groups per gram of nanotubes much higher than that of alkyne moieties, as calculated from TGA experiments. The field-dependent magnetization curve of **CNT-IO 1** showed a superparamagnetic behaviour at 300 K. Besides, the saturation magnetization value of this

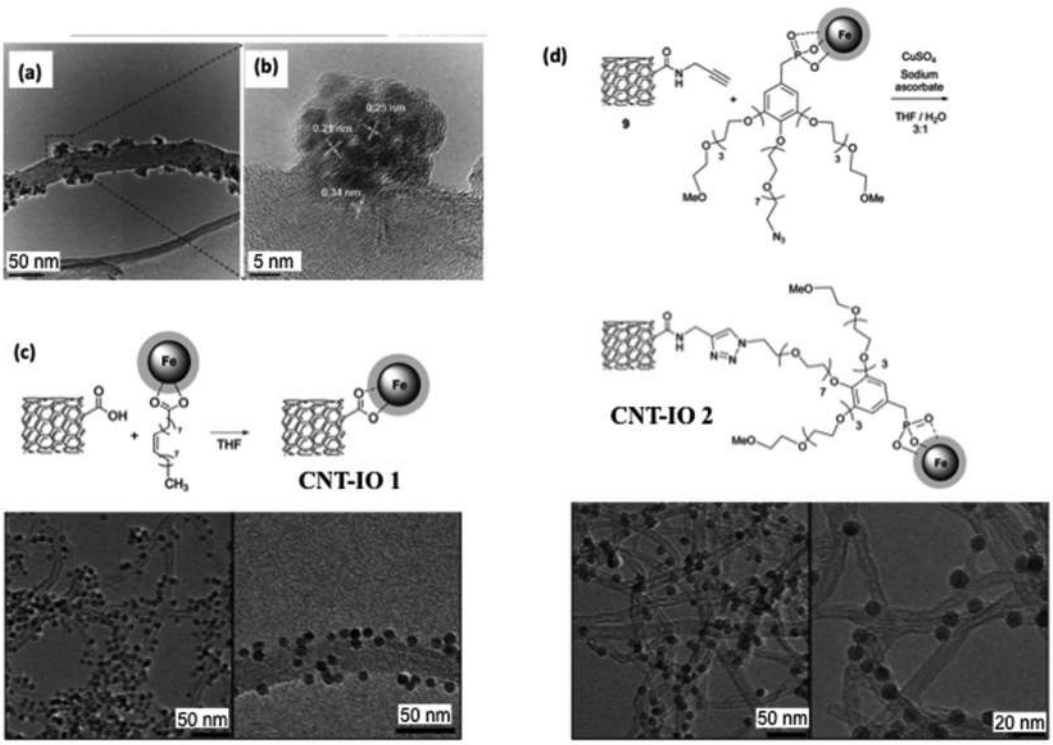

Fig. 5 (a), (b) TEM and HRTEM images of hydrophilic MWCNT/Fe_3O_4 hybrids showing iron oxide nanoparticle clustering on the surface of the CNTs. Reprinted from ref. 54, H. Wu *et al.*, The behavior after intravenous injection in mice of multiwalled carbon nanotube/Fe_3O_4 hybrid MRI contrast agents, *Biomaterials*, 2011, **32**, 4867–4876, Copyright 2011, with permission from Elsevier. (c), (d) Ligand exchange and click chemistry ligation strategies for the synthesis of CNT–iron oxide nanoparticle hybrids. Reproduced from ref. 57 with permission from The Royal Society of Chemistry.

CNT–IO hybrid was practically the same as that of NPs alone (53 emu g^{-1} *vs.* 52 emu g^{-1}).[58] This indicates that the magnetic properties of the iron oxide nanoparticles are maintained after their conjugation to the CNTs. The authors evaluated the potential of **CNT-IO 1** as a contrast agent for MRI (see section 3); however, they did not conduct a further systematic investigation of the magnetic properties and potential biological applications of both magnetic CNT hybrids. Therefore, a direct comparison of their magnetic properties and interaction with cells and how these are affected by differences in the density and homogeneity of the surface coverage with NPs is not within reach.

Nature offers a large diversity of structures able to function as biological templates for the synthesis of anisotropic magnetic nanomaterials. Among biomolecules, DNA has been extensively used as a soft template to assemble 1D magnetic nanostructures. Byrne *et al.* prepared magnetite nanowires using herring sperm DNA (hs-DNA).[59] The nanowires were assembled *in situ* from spherical Fe_3O_4 nanoparticles with a diameter of 9 ± 2 nm, obtained by co-precipitation of Fe(II) and Fe(III) salts in the presence of DNA. Interestingly, the use of double-stranded DNA induced the formation of entangled chains, while heat-denatured DNA (single-stranded) promoted a more ordered assembly (Fig. 6a and 6c). Under the influence of an external magnetic field oriented perpendicular to the samples, a further alignment of the single-stranded DNA-magnetite chains was observed, resulting in the formation of ropes with lengths of several microns (Fig. 6b). By contrast, the morphology of the double-stranded DNA-magnetite nanoconstructs was not affected by the exposure to an external magnetic field (Fig. 6d). These DNA-magnetite hybrids showed an unusual magnetic behaviour, with very high longitudinal (r_1) relaxivity at low magnetic fields, especially in the case of the single-stranded constructs. This behaviour is completely unexpected for pure superparamagnetic samples and was attributed to the more ordered aggregation of the NPs along the single-stranded DNA scaffold.

Ivanisevic and co-workers reported several examples of DNA-templated hybrid nanoparticle chains starting from individual spherical gold, iron oxide and/or cobalt iron oxide

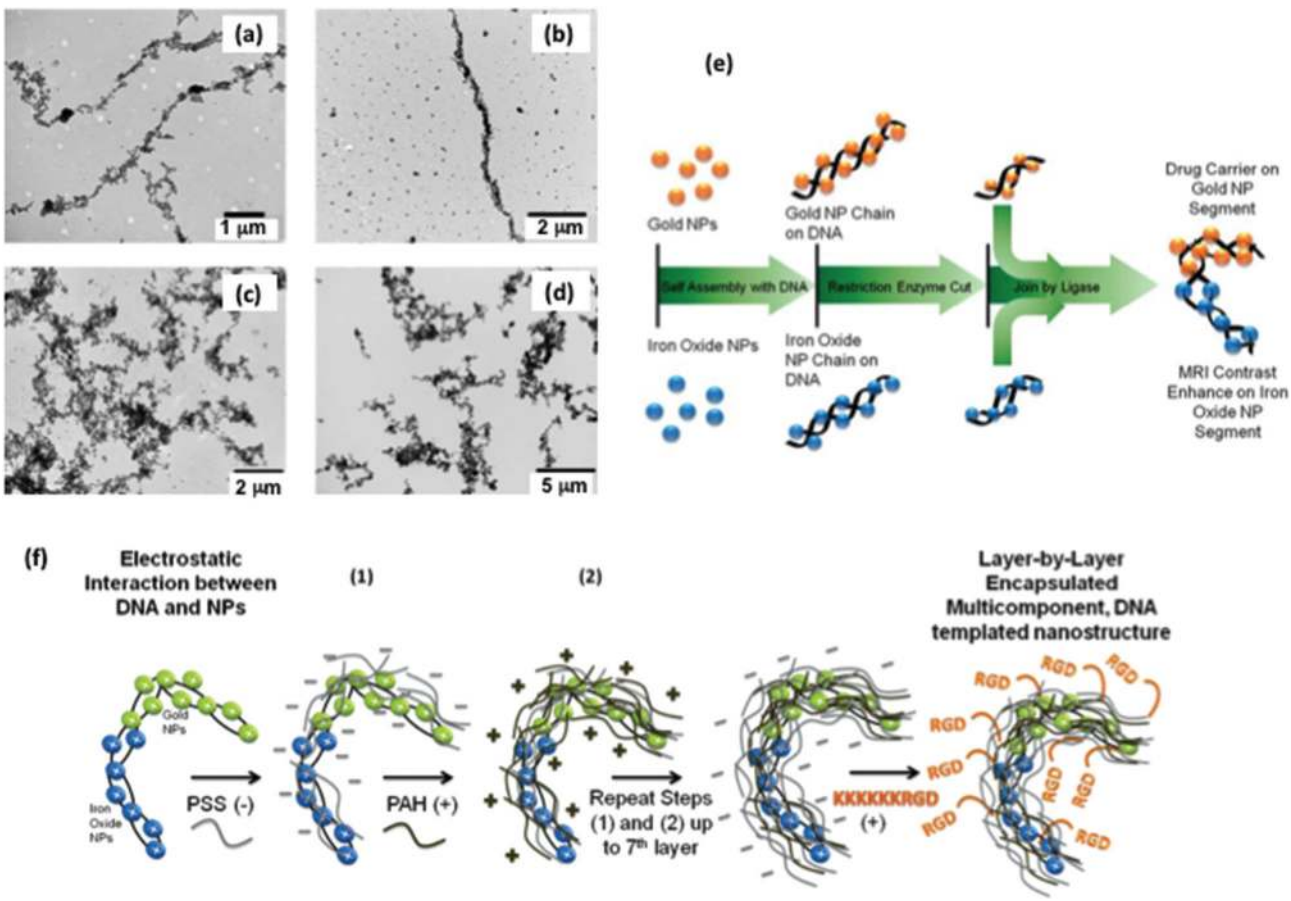

Fig. 6 Anisotropic magnetic nanomaterials created using DNA templates. TEM images of magnetic nanowires assembled on single-stranded (top) and double-stranded (bottom) herring DNA in the absence (a, c) and in the presence of an external magnetic field (b, d). Reproduced from ref. 59 with permission from The Royal Society of Chemistry. (e) Schematic representation of the fabrication of Au-magnetic nanoparticle chains on DNA. (f) Layer-by-layer encapsulation of multicomponent Au–iron oxide nanochains. Reproduced from ref. 65 with permission from The Royal Society of Chemistry and ref. 60, Copyright 2010, American Chemical Society.

nanoparticles.[60–65] The method employed to construct the DNA-nanoparticle hybrids is summarized in Fig. 6e. In the first step, positively charged nanoparticles were self-assembled using the negative backbone of DNA and then the chains were cut into shorter strands by the action of restriction enzymes such as EcoRI. For the construction of multicomponent chains, Au and magnetic short strands were joined together using a ligase. To enhance their cellular uptake, the resulting chains were further encapsulated using a layer-by-layer (LBL) approach (Fig. 6f), in which negatively and positively charged polymers were alternatively wrapped around the chains and the outermost polymer layer was decorated with targeting ligands such as RGD peptides. This system presents several advantages, as it requires relatively cheap starting materials, is performed at room temperature in aqueous media and allows for a flexible design of the components. Moreover, a multifunctional platform for biological applications can be created, by combining the MRI contrast enhancement induced by the magnetic NP component with controlled drug delivery from the Au NP segment. Another remarkable feature of this design is the fact that the chain lengths and the amount of magnetic nanoparticles (which is ultimately responsible for the contrast in MRI) can be fine-tuned through the synthesis.[62] In all their studies, the authors observed increased transverse relaxivity values for the DNA-NP chains when compared to spherical single components. Interestingly, although in general the LBL encapsulation of the DNA-NP chains led to a decrease in the transverse relaxivity in water and MRI phantoms, this difference was not significant for 3D cell culture phantoms (see section 3.5). In this case the contrast in MRI was given by the amount of contrast agents internalized by cells; therefore the improved cellular uptake of the encapsulated chains could be responsible for the observed results.[64] Although the anisotropy clearly induced better magnetic properties, the authors reason that in this case the cell internalization was improved by the presence of targeting ligands on the chains, rather than by the shape of the nanostructure.

2.2 Assembly methods

One-dimensional assemblies of magnetic nanoparticles can be obtained in a variety of ways, the most common being magnetic dipole–dipole interaction, self-assembly processes (usually mediated by polymers) and covalent chemical linkage. In many cases a cooperative combination of an external magnetic field (to pre-align the nanoparticles) and a polymer (to act as a linker and hold the nanoparticles together in a linear chain-like conformation) is used. An evident advantage of some assembly methods (such as zero-field assembly and covalent linkage) over direct synthesis is the fact that the diameter of the resulting high aspect ratio nanomaterial is dictated by the diameter of the individual building blocks, enabling the construction of materials with diameters down to a few nanometres. On the other hand, the synthetic procedures can be sometimes cumbersome and might require additional synthetic steps and/or advanced functionalization of the individual nanoparticles.

2.2.1 Magnetic assembly

Zero-field assembly. The formation of linear chains in the absence of an external field if magnetic dipole–dipole interactions between individual nanoparticles are sufficiently strong was predicted more than three decades ago by theoretical calculations.[66] This linear assembly is expected when the dipolar coupling constant λ, which depends on the size of the nanoparticle, has values superior to 2. However, direct evidence of the existence of such magnetic structures was not provided until the early 2000s, when Philipse and co-workers reported cryo-TEM images of magnetite chains assembled under zero-field conditions from individual 21 nm spherical nanoparticles (Fig. 7a and b).[67] The authors clearly demonstrated that the driving force for the assembly was the dipolar interaction between nanoparticles, which depends on the size of the nanoparticles. While 21 nm nanoparticles ($\lambda \approx 7$) assembled in linear chains, 16 nm nanoparticles ($\lambda \approx 2$) formed only droplet-shaped aggregates.

Meng *et al.* obtained highly uniform 1D magnetic nanochains following a simple, one-pot procedure using $FeCl_3$, sodium oleate and standard surfactant molecules (oleic acid and oleylamine).[68] The nanochains were composed of polyhedron-shaped α-Fe_2O_3 nanoparticle units with an average diameter of 19.8 nm and excellent uniformity (Fig. 7c). A close look at the contact region between two contiguous nanoparticles by high-resolution TEM (HRTEM, Fig. 7d) and the corresponding reversed-phase fast-Fourier-transform (FFT) pattern demonstrated the single-crystal nature of the junction area. The authors reasoned that in the initial stages of the synthesis (when the concentration of the precursors is high), metastable polyhedron-shaped particles stabilized by capping of oleic acid and oleylamine on their surface are formed under a kinetic growth regime. These initial nanocrystals have a high free energy, especially when looking at the atoms located at their corners. As the reaction proceeds, the concentration of the precursors decreases and further evolution of the nanoparticles into chains is governed by the minimization of the overall surface energy: atoms might migrate from higher energy positions to lower ones, thus causing the transition areas to dissolve and promoting the linear growth of the nanochains (Fig. 7e). A similar process was observed by Palchoudhury *et al.* during the thermal decomposition of iron oleate in the presence of a weakly bound surfactant, trioctylphosphine oxide (TOPO).[69] Time-dependent studies revealed that spherical maghemite nanoparticles are formed at short reaction times (1 h), whereas at longer reaction times these aggregate into high aspect ratio structures (nanoworms) with the same diameter (12 nm) as the spherical nanoparticles.

Jia *et al.* reported a rapid and economical procedure for the synthesis of $FeNi_3$ nanochains by reduction of Fe(III) and Ni(II) precursors in the presence of hydrazine and under microwave irradiation.[70] Several parameters were found to play a key role in the process: a moderate microwave intensity was necessary to ensure the growth of magnetic nanochains of high purity, while the diameter of the nanoparticles (and therefore the diameter of the chains) could be controlled by adjusting the

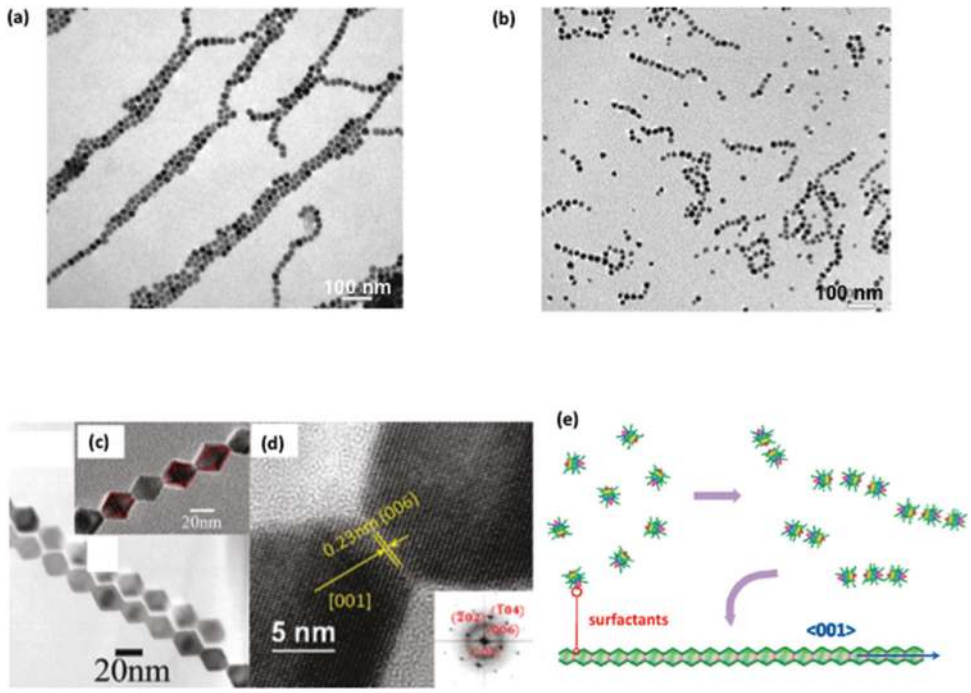

Fig. 7 Representative TEM (a) and cryoTEM (b) images of 21 nm magnetite nanoparticle chains assembled under zero-field conditions. Reprinted with permission from ref. 67. Copyright 2004, American Chemical Society. (c) and (d) TEM image of maghemite nanochains and representative HRTEM picture of the contact area between two contiguous nanoparticles and the corresponding FFT pattern. (e) Proposed mechanism for the growth of the nanochains. Reprinted with permission from ref. 68. Copyright 2010, American Chemical Society.

concentrations of the Fe and Ni precursors. The nanochains revealed a ferromagnetic behaviour and their saturation magnetization was found to be 350 times higher than that of the corresponding spherical $FeNi_3$ nanoparticles. The authors reasoned that the anisotropic structure of the chain was at the origin of this behaviour. However, none of the synthetic procedures discussed in ref. 68-70 attributes the chain formation to the magnetic dipole–dipole coupling mentioned by Philipse. Therefore, it is difficult to establish a size limit below which individual NPs cannot self-assemble into chain-like structures without the aid of an external magnetic field.

Magnetic-field-induced assembly. Magnetic-field-induced (MFI) assembly of nanoparticles is one of the most widely exploited routes for the fabrication of ordered structures (for detailed overviews of the subject, see the reviews of Yin and co-workers[71,72]). The initial building blocks can be synthesised *in situ* or in a previous synthetic step. Many MFI assembly procedures employ polymers to "glue" together the nanoparticles by electrostatic interactions. These examples will be discussed in this section and not in section 2.2.2, where we will cover encapsulation in polymers as a stand-alone method to generate magnetic anisotropic structures.

Sheparovych *et al.* used magnetic field-induced assembly to construct magnetite nanowires.[73] Superparamagnetic spherical nanoparticles capped with citric acid (which provides them with a negative surface charge) were linked together using a positively charged polyelectrolyte, poly(2-vinyl-*N*-methylpyridinium iodide). The reaction was carried out inside a plastic cell mounted on top of a magnet; in a control experiment performed in the absence of an external magnetic field, only random arrays of iron oxide nanoparticles were observed by TEM. VSM measurements demonstrated that the nanowires preserved the superparamagnetic properties of individual building blocks.

Electrostatic interactions between magnetic nanoparticles and polymers can be exploited to construct colloidal assemblies, as shown by Berret and co-workers. In a first study, rod-like structures were assembled by mixing solutions of poly(trimethylammonium ethylacrylate methylsulfate)-*b*-poly(acrylamide) and polyacrylic acid-coated maghemite nanoparticles and dialysing the resulting mixture under a constant magnetic field of 0.1 T.[74] It is noteworthy that when the dialysis was carried out in the absence of a magnetic field, only spherical aggregates were obtained. Once again, the high aspect ratio nanostructure maintained the superparamagnetism of the spherical nanoparticles. This methodology was extended to the preparation of bimodal superparamagnetic–fluorescent nanorods assembled from anionic iron oxide and organic fluorescent nanospheres in the presence of a cationic block copolymer.[75] A comprehensive study on the cellular uptake, toxicity and degradation of magnetic nanowires assembled from γ-Fe_2O_3 nanoparticles and poly(trimethylammonium ethylacrylate)-*b*-poly(acrylamide) was further reported by the same group (see section 3).[76]

Fragouli *et al.* reported on the use of MFI to create nanocomposite polymeric (poly(ethylmethacrylate-*co*-methylacrylate), PEMMA) films incorporating nanowire arrays of γ-Fe_2O_3 nanoparticles of 10 nm mean diameter.[77] The nanowires retained the superparamagnetism of the spherical nanoparticles and presented magnetic anisotropy. Magnetization values measured with a magnetic field parallel to the nanowires were higher than that when the field was oriented perpendicular to the wires, consistent with previous reports of Sahoo *et al.*[78] and Sheparovych *et al.*[73] In a follow-up study, the same authors reported a theoretical investigation of the aggregation of individual spherical superparamagnetic nanoparticles under the influence of an external magnetic field.[79] The study was conducted for 11 and 17 nm iron oxide nanoparticles capped with oleic acid, using a Monte Carlo method. Simulations were carried out both in the absence and in the presence of a magnetic field and predicted a much clearer aggregation tendency for the bigger particles. The formation of chains starting from 10 nm nanoparticles, observed in their previous work,[77] was attributed to the presence of the polymer, which can reduce inter-particle electrostatic interactions and favour the aggregation into clusters. Moreover, from Monte Carlo simulations of SQUID experiments with parallel and perpendicular orientations of the applied magnetic field a ratio between parallel and perpendicular magnetization of 2.5 ± 1.1 for the 11 nm nanoparticles was calculated, in line with the experimental value of 1.9 ± 0.3 obtained for the chains of 10 nm iron oxide nanoparticles.

Yin and co-workers reported the synthesis of responsive photonic nanochains composed of superparamagnetic Fe_3O_4 colloidal nanocrystals (CNCs)[80] using a sol–gel synthesis assisted by an external magnetic field.[81] The process is schematically described in Fig. 8a. The key step is the application of an external magnetic field for a short period of time during the silica coating to induce the assembly of the individual nanoparticles into chains, which were further coated with an additional silica layer for stability purposes. The procedure yields robust chain-like structures, persistent after the removal of the magnetic field (Fig. 8b); moreover, it allows a high degree of control over the structural features of the chains. By fine-tuning the exposure time to the magnetic field the authors were able to control the length of the chains, while adjusting the time-points of magnetic exposure enabled control over the interparticle distance. These magnetically responsive photonic nanochains could find applications in biosensing.

Not only individual magnetic nanoparticles, but also small clusters of NPs can be assembled into ordered chains by applying an external magnetic field, as shown by the work of Wang *et al.*[82] In this approach, nanoclusters with an average

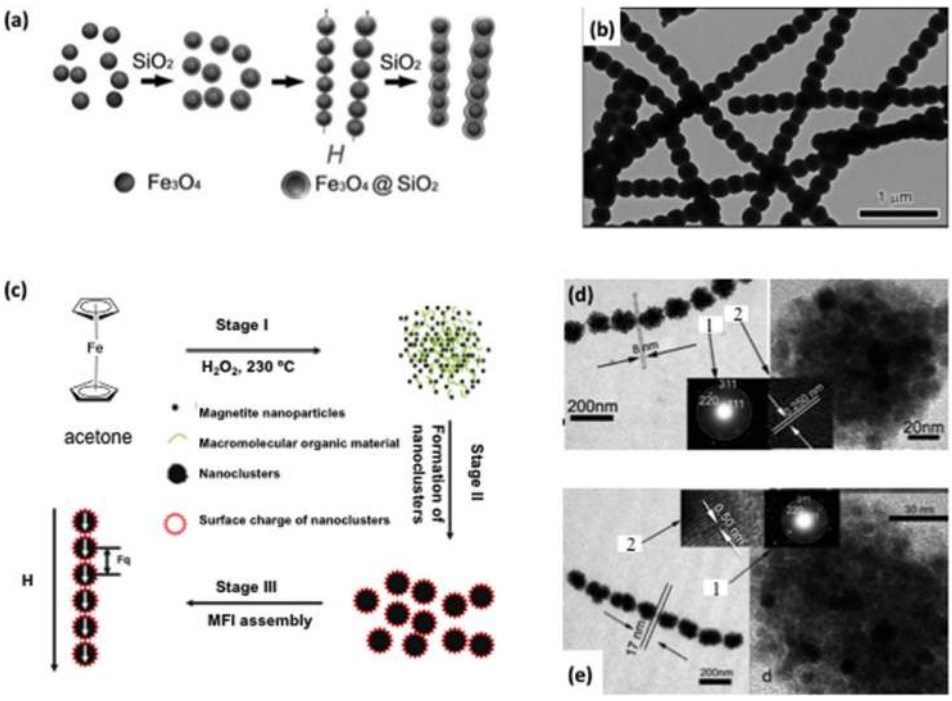

Fig. 8 (a) Schematic illustration of the fabrication of 1D nanochains of Fe_2O_3 nanoparticles by aggregation in the presence of an external magnetic field *H*. (b) Representative TEM image of 1D nanochains. Reprinted with permission from ref. 81 with permission from John Wiley & Sons. (c) Formation mechanism for nanochains composed of clusters of magnetic nanoparticles. Stage I: thermal decomposition of ferrocene; stage II: formation of clusters; stage III: chain assembly under the influence of the external magnetic field. (d) and (e) TEM images of chains with different intercluster spacings (1 and 2 in the insets indicate electron diffraction pattern and lattice fringe, respectively). Reprinted with permission from ref. 82. Copyright 2009, American Chemical Society.

diameter of 120 nm were synthesised starting from ferrocene and then assembled into chains using an external magnetic field (Fig. 8c). The length of the chains was affected by the magnetization time, with practically all the individual NPs assembled into chains after 16 h of exposure to the external magnetic field. The strength of the magnetic field had a clear influence on the formation of highly ordered structures, as the application of a magnetic field of 0.2 T resulted in a much more ordered chain than that of 0.1 T. Finally, the amount of hydrogen peroxide used for the synthesis of the spherical NPs influenced not only the distance between adjacent nanoclusters in the chains, but also the chemical composition of the nanoparticles. A molar ratio of H_2O_2–ferrocene of 40 : 1 produced pure magnetite nanoparticles assembled in chains with an intercluster distance of 8 nm (sample **S1**, Fig. 8d). However, when the amount of H_2O_2 was doubled the resulting nanoparticles consisted of a mixture of maghemite, magnetite and hematite and the spacing between adjacent clusters increased to 17 nm (sample **S2**, Fig. 8e). The authors postulated that the shorter intercluster distance in the sample that contained only magnetite clusters could be explained by a stronger attraction between the nanoparticles. This was reflected in the saturation magnetization values, which were slightly higher for sample **S1** (55 emu g^{-1}) than for sample **S2** (46 emu g^{-1}). Based on the fact that individual nanoparticles were smaller than 20 nm and therefore superparamagnetic, the authors predicted a similar magnetic behaviour of the nanochains. However, magnetic measurements revealed a weak ferromagnetic character of the chains. This transition from superparamagnetism to ferromagnetism was attributed to the formation of 1D chains,[83] showing how shape anisotropy can be used to manipulate the magnetic properties of the material.

2.2.2 Self-assembly

Polymer-assisted assembly. Polymers are commonly used in the synthesis of magnetic nanomaterials for stabilisation and biocompatibility purposes. However, they can also play a significant role in tuning the morphology and magnetic properties of the obtained nanomaterials. By controlling the ratio between maleic anhydride grafted polypropylene (PP-*g*-MA) and the iron precursor ($Fe(CO)_5$), Wei and co-workers obtained superparamagnetic α-Fe_2O_3 hollow spheres (weight ratio PP-*g*-MA/Fe(CO)5 = 1 : 3.5), or ferromagnetic nanowires composed of core–shell γ-Fe_2O_3 nanoparticles when the ratio of PP-*g*-MA/Fe(CO)5 was changed to 1 : 14.[84] The authors explained the nanowire formation by a self-assembly process driven by magnetic dipole–dipole interactions between nanoparticles and van der Waals forces between the surrounding polymer molecules. More recently, the same group demonstrated that by changing only the molecular weight of polypropylene grafted with terminal maleic anhydride (PP-MA) it is possible to control the structure, size and morphology of the individual iron oxide building blocks, as well as the magnetic properties of the resulting nanochains.[85] When using a low molecular weight polymer (M_w = 2500 Da), thermal decomposition of $Fe(CO)_5$ resulted in nanochains composed of spherical γ-Fe_2O_3 nanoparticles of 24 nm diameter and showing a ferromagnetic "hard" character (coercivity of 292.7 Oe). By contrast, nanochains with a ferromagnetic "soft" behaviour (coercivity of 70.5 Oe) were assembled from slightly bigger (30 nm diameter) flower-like γ-Fe_2O_3 nanoparticles in the presence of a higher molecular weight PP-MA (M_w = 8000 Da). The different morphology of the nanoparticles was attributed to the different capping strengths of the polymers, which are directly related to the density of maleic anhydride groups. These act as capping ligands for the nanoparticles in a similar fashion to typical carboxylic acid ligands. Since the mass of polymer used is the same for both syntheses (0.25 g), for the 8000 Da PP-MA less maleic anhydride groups were available in the reaction medium, inducing the growth of small flower-like clusters of NPs. When 2500 Da PP-MA was used only individual spherical nanoparticles were formed because of a stronger capping. Importantly, this one-pot colloidal synthesis enabled gram-scale production of such magnetic colloids with potential sensing applications.

In 2008 Sailor and co-workers reported the first example of iron oxide "nanoworms" (NWs) synthesised by a modified co-precipitation method using higher Fe(II) and Fe(III) salt concentrations and 20 kDa molecular weight dextran to induce the linear assembly of 5–10 iron oxide cores.[4] Although the authors did not carry out an in-depth study of the aggregation mechanism, they suggest that the key factor was the molecular weight of the polymer. Their reasoning was based on the fact that highly branched structures with a broader size distribution were obtained when 40 kDa molecular weight dextran was used, while 10 kDa dextran typically promotes the formation of spherical nanoparticles.[86] The nanoworms displayed slightly higher saturation magnetization than their spherical counterparts, as well as higher transverse relaxivity values, demonstrating the effect of the shape anisotropy on their magnetic properties. A further investigation of the magnetic properties of the nanoworms revealed that their transverse relaxivity increased linearly with the magnetic field, which indicated that they could find promising applications as MRI contrast agents.[18] As a matter of fact, these nanoconstructs represent one of the most prolific examples of anisotropic magnetic nanoparticles with biomedical applications (see section 3).

Corr *et al.* reported the synthesis of linear assemblies of magnetite nanoparticles prepared by co-precipitation of $FeCl_3{\cdot}6H_2O$ and $FeCl_2{\cdot}4H_2O$ in the presence of a polyelectrolyte (poly(sodium-4-styrene sulfonate), PSSS), at different Fe : monomer ratios (1 : 2, 3 : 1, 6 : 1).[17] The polyelectrolyte acted both as a stabilising agent, its negatively charged backbone promoting the aggregation of positive Fe ions, and as a template by directing the assembly of the resulting iron oxide nanospheres into chain-like structures. The chain-like morphology was observed by TEM when the samples were dried in the absence of an external magnetic field; however, upon drying in a 0.5 T magnetic field these linear chains further aligned to form parallel arrays of wire-like structures. The authors also reported preliminary results regarding the potential use of these nanocomposites as MRI contrast agents (see section 3).

Liu and co-workers reported a two-step route to synthesise superparamagnetic anisotropic structures ("nanoworms") by precipitation polymerization of divinylbenzene (DVB) in the presence of previously synthesised 10 nm oleic acid-coated Fe_3O_4 nanoparticles.[87] The elongated structures were not formed by individual nanoparticles, but by clusters of approximately 80–100 nm. The authors proposed a mechanism in which Fe_3O_4–PDVB nanocomposites were formed at an initial stage, followed by aggregation probably due to magnetic dipole–dipole interactions. The nanoworms showed superparamagnetic behaviour at room temperature, but ferromagnetism at 5 K. Although the authors envisaged possible applications for drug delivery and MRI, no further studies were conducted to this end.

Self-assembly of amphiphilic nanoparticles. In a recent report, Bishop and co-workers showed that gold amphiphilic nanoparticles functionalized with hydrophobic and hydrophilic ligands can self-assemble into short chains in which the particles are held together by hydrophobic interactions.[88] This self-assembly takes place if the nanoparticles have an "adaptive" surface chemistry, with ligands that are not bound in an irreversible manner to the NP surface and are able to rearrange during the assembly process in order to minimize the number of hydrophobic ligand–water contacts. By adjusting the amount of hydrophobic ligands, the preferred coordination number of the nanoparticles could be varied from 1 (dimers) to 2 (linear chains) and 3 (clusters); moreover, high salt concentrations were necessary for the formation of chains (most likely by limiting repulsive electrostatic interactions only to the nearest neighbours). This controlled self-assembly was further extended to obtain linear chains of 8 nm superparamagnetic $CoFe_2O_4$ nanoparticles functionalized with hydrophobic (1,2-hexadecanediol, HDD) and hydrophilic (10,11-dihydroxyundecanoic acid, DHUA) ligands. At a HDD ligand coverage fraction of 0.2, these nanoparticles assembled into linear chains, as revealed by cryo-TEM images. The authors reasoned that the formation of chains could not be attributed to magnetic dipolar interactions between the $CoFe_2O_4$ nanoparticles because at this particle size the strength of dipole–dipole interaction is not sufficient to promote a magnetic assembly. Therefore, the chain formation was explained by hydrophobic interactions between the HDD ligands. This hypothesis was confirmed by the fact that no chains were observed in the absence of HDD.

2.2.3 Covalent chemical linkage. Selective functionalization of nanoparticle surfaces can enable the construction of anisotropic structures *via* covalent bond formation. Peiris *et al.* used a solid-phase synthesis strategy to obtain iron oxide nanospheres with asymmetric surface chemistry, which were further assembled into linear chains in a controlled fashion (Fig. 9a).[89] Amine-modified iron oxide nanoparticles were attached to a solid phase functionalized with a homobifunctional cleavable cross-linker containing disulfide bonds; cleavage from the resin yielded nanoparticles with asymmetric surface functionalization. The procedure was repeated until reaching the desired chain length. This methodology, although more time consuming, allows a good control over the length and aspect ratio of the nanochains and could be extended to the preparation of hybrid nanostructures (*e.g.* chains assembled from iron oxide nanoparticles and liposomes[90]). Another interesting feature is the fact that the partially modified area (PMA, the area capable of binding to a solid support) of the nanoparticle depends on its size, as well as on the length of the linker and the polymer chosen as tether. This provides excellent flexibility and the ability to fine-tune the surface asymmetry according to a rational design. The nanochains outperformed their constituting spherical components in terms of magnetic properties. For instance, a nanochain composed of three 30 nm spheres showed a 2.25-fold increase in the value of transverse relaxivity at 1.4 T.

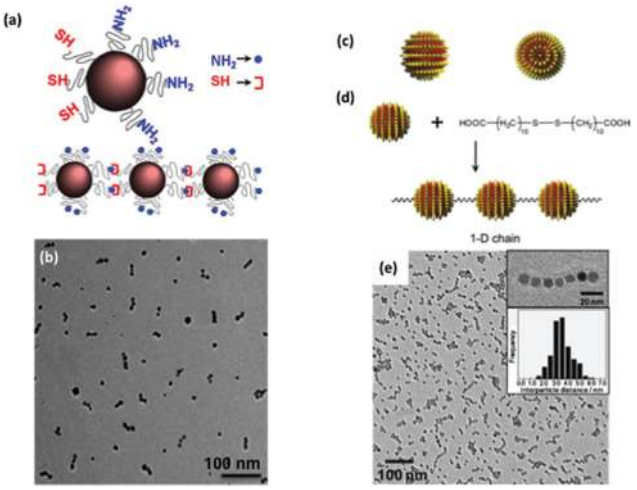

Fig. 9 Covalent nanoparticle chains. (a) Nanospheres with asymmetric surface chemistry assembled into nanochains by solid-phase synthesis. (b) Representative TEM image of the nanochains. Reprinted with permission from ref. 89. (c) Side-view and top-view of rippled γ-Fe_2O_3 nanoparticles coated with mixed ligands. (d) Formation of 1D chains by reaction of the nanoparticles with the molecular linker and TEM picture of the chains (e). Reprinted from ref. 91 with permission from John Wiley & Sons.

In a very elegant approach, Stellacci and co-workers created covalent chains of superparamagnetic iron oxide nanoparticles by taking advantage of polar point defects present on the surface of γ-Fe_2O_3 nanoparticles capped with two different ligands (nonanoic acid and 4-phenylbutyric acid).[91] In their previous work, the authors showed that when spherical gold nanoparticles were coated with two ligands of different lengths, they arranged in a unique rippled fashion on the surface of the nanoparticle, resulting in striated domains (Fig. 9b).[92] This arrangement generates two diametrically opposed point defects that can be used for place-exchange reactions with molecular linkers to create 1D chains of nanoparticles[92,93] and is independent of the nature of the metallic core, as demonstrated further for iron oxide nanoparticles. When the mixed-ligand coated γ-Fe_2O_3 nanoparticles were reacted with a bifunctional linker, 11-(10-carboxy-decyldisulfanyl)-undecanoic

acid (Fig. 9c), chains with an average length of 4 nanoparticles (≈100 nm) were observed by TEM (Fig. 9d). The authors demonstrated the covalent nature of the chains by performing several control experiments. No chains were formed in the absence of the linker or when a monofunctional linker was used; importantly, the reaction of the linker with homoligand capped γ-Fe_2O_3 nanoparticles also did not yield chains of nanoparticles, since such nanoparticles lacked the ripple structure that generates the point defects. Moreover, because of the size of the nanoparticles the formation of the chains *via* magnetic dipole–dipole interactions was also ruled out, as this mechanism would require larger nanoparticles; see the discussion in section 2.2.1. The chains showed superparamagnetic behaviour at room temperature and a larger increase in their magnetization at increasing applied magnetic field when compared to isolated spherical nanoparticles.

3. Biomedical applications

As already mentioned in the Introduction section, anisotropic nanomaterials are expected to have a different interaction with biological systems than their spherical analogues. The biological applications of high aspect ratio magnetic nanomaterials, although less numerous than those of spherical magnetic nanoparticles, have often shown clear advantages that were related to their anisotropic properties. It is reasonable to assume that once we will manage to develop more general, robust, effective and high-scale synthetic methods, the use of these nanomaterials in biomedicine will become more widespread.

3.1 Surface functionalization

Chemical modification of the surface of nanomaterials is essential for providing them with the desired biological functionality and for ensuring their biocompatibility and stability in physiological media. Nanomaterials designed for biomedical applications must be able to overcome several biological barriers before reaching their target and must preserve the properties of the inorganic core and the attached biomolecules. Although our understanding regarding the biological fate of nanomaterials has improved significantly over the last decade, there are still many unknown aspects related to the toxicity of nanomaterials and their interaction with biological entities.

A detailed discussion regarding the biofunctionalization of nanomaterials is outside the scope of the present review. Therefore, in this section we briefly address some key issues and we provide more details when presenting the biomedical applications of high aspect ratio magnetic nanomaterials. For exhaustive revisions we direct the reader to a number of relevant literature reviews on the topic.[16,94–103]

There are several important aspects to be taken into account when considering the interaction of nanomaterials with living systems (Fig. 10).[100] Appropriate coating of nanoparticles is crucial in order to prevent adverse effects related with adsorption of serum proteins (opsonization). This protein

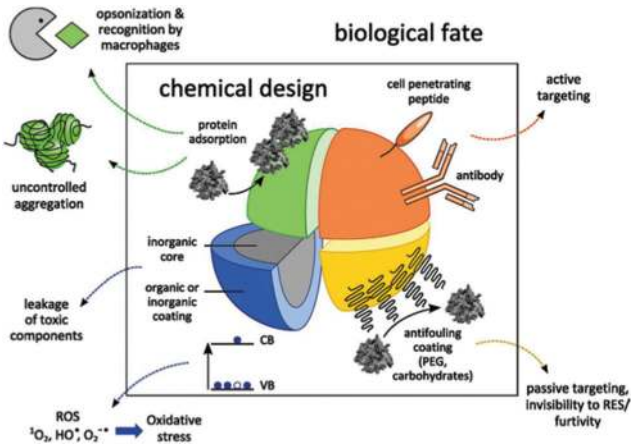

Fig. 10 Overview of nanomaterial–biological entities interactions and tips for functionalization. Green: protein adsorption can induce aggregation and promote recognition by the immune system. Blue: potential toxic effects associated with decomposition of the nanomaterial. Orange: surface functionalization for active targeting. Yellow: surface passivation to avoid recognition and clearance by the immune system. Reprinted from ref. 100 with permission from John Wiley & Sons.

adsorption represents the first immune response of the body and can lead to aggregation of nanoparticles and to their subsequent recognition by phagocytes. Surface coating with passive targeting elements such as biocompatible polymers and carbohydrates can also act as a "shield" to render the nanoparticles invisible to the immune system, thus increasing their blood circulation time. Importantly, coating provides functional groups for anchoring therapeutic and active targeting elements (*e.g.* antibodies, cell-penetrating peptides or tumour targeting units). Last but not least, potential cytotoxic effects of nanomaterials can also be related to their surface functionalization. On the one hand, coating can improve the biocompatibility of nanomaterials and prevent leakage of inorganic or organic cytotoxic elements. On the other hand, however, certain types of coating materials can enhance toxicity. Nanomaterials containing cationic polymer coatings have generally shown higher *in vitro* toxicity than neutral or anionic ones. Their cytotoxic effects range from defects in lipid membranes to cell lysis, apoptosis and necrosis and have been associated with higher extent of cell internalization of cationic nanomaterials.

3.2 Interaction of high aspect ratio magnetic nanomaterials with living systems: cellular uptake, biodistribution and toxicity aspects

To date, information concerning cellular uptake mechanisms, cytotoxicity, biodistribution and degradation of magnetic anisotropic nanomaterials is rather limited when compared to spherical nanoparticles. Given the broad size distribution of high aspect ratio magnetic nanomaterials, with lengths ranging from a few tens of nanometres to several micrometres, it is even more difficult to generalize and predict the way they

will interact with living entities. Some early studies suggested that Ni magnetic nanowires were internalized by fibroblast cells following the integrin-mediated phagocytosis pathway and established that the cellular uptake was maximized when the length of the nanowires matched the diameter of the cells.[41] Likewise, Song *et al.* proposed that the mechanism of uptake of iron nanowires by HeLa cells depends on the length of the nanomaterial.[104] Short nanowires with lengths between hundreds of nanometres to a few micrometres were most likely internalized by non-specific pinocytosis, while longer nanowires could perforate the cell membrane and diffuse through it in a similar way to that reported for carbon nanotubes.[105] Cytotoxicity assays revealed that the Fe nanowires were generally benign to the cells, only showing a slight cytotoxic effect at increased concentrations and upon prolonged exposure times. Magnetic Ni nanowires reported by Chen and co-workers[106] also showed little to no toxicity when internalized by fibroblasts, as inferred from an assessment of gene expression of IL-6 (a pro-inflammatory cytokine that is upregulated in fibroblasts as a result of trauma), as well as from MTT (3-(4,5-dimethylthiazol-2-yl)-2,5-diphenyl tetrazolium bromide) cell viability assays. However, magnetic actuation on the internalized nanowires by the application of an external magnetic field could induce cell death by disrupting the intracellular environment.

McCarthy *et al.* demonstrated that the cellular uptake of magnetic-fluorescent nanowires was dependent not only on their aspect ratio, but also on the surface functionalization.[48] Plain polystyrene-coated wires showed practically no interaction with A549 cells, as opposed to nanowires functionalized with anti-ICAM-1 (intracellular adhesion molecule 1) antibodies. Depending on their lengths, these were either internalized ("short" nanowires with aspect ratio <50) or attached to cell membranes by binding to the ICAM-1 surface receptor ("long" wires, aspect ratio >50). Similarly, short (2.6 μm) Au-coated Ni nanowires functionalized with polyethylene glycol and glutathione were internalized by macrophage RAW 264.7 cells, most likely *via* phagocytosis.[47] These nanowires showed good biocompatibility, as demonstrated by a comprehensive cell viability study carried out on several cell types. Non-coated Ni nanowires generally displayed higher cytotoxicity than Au–Ni nanowires; however, in this study the concentration of the Ni nanowires was much higher than the lethal concentration of similar 20 μm Ni nanowires,[42] indicating the importance of tailoring the length to increase the biocompatibility of such aspect ratio nanomaterials. Although in general an appropriate polymer coating is required to ensure the biocompatibility of nanomaterials, bare $FeNi_3$ nanochains synthesised by Jia *et al.* showed very low *in vivo* cytotoxicity in zebrafish larvae, with more than 90% survival even after 96 h of exposure at concentrations of 50 mg L^{-1}.[70]

Perhaps the most representative examples of how the surface functionalization in combination with the shape anisotropy can influence cell internalization can be found in the work of Sailor and co-workers.[4,5] In a proof of principle study, iron oxide nanoworms decorated with multiple copies of fluorescent cell-penetrating peptide F3, which is known to selectively target cell-surface receptors in tumour cells, showed increased cellular uptake in MDA-MB-435 human carcinoma cells when compared to F3-functionalized nanospheres (Fig. 11a). Moreover, cell uptake did not affect the nanoworm shape, as demonstrated by TEM analysis of the nanomaterials recovered both from cells and from the bloodstream after 24h. Although both nanospheres and nanoworms showed similar blood circulation times (15–18 h) and biodistribution in mice, the nanoworms were eliminated from tumours much slower than the nanospheres, indicating their potential to function as more effective delivery and/or imaging agents. In a more systematic work, the same authors explored different targeting elements (positively charged F3 peptide recognising cell surface *vs.* neutral CREKA peptide that targets clotted plasma proteins in tumours), peptide surface coverage and functionalization chemistry (longer PEG *vs.* shorter sulfo-SMCC linkers) and shape (nanoworms *vs.* nanospheres) for the targeting of two types of mouse xenograft tumours (MDA-MB-435 human carcinoma and HT1080 human fibrosarcoma) (see Fig. 11b).[5] Elongated structures demonstrated again their superiority in terms of *in vivo* tumour targeting ability and blood half-life, while the smaller CREKA peptide was found to be more effective than F3 for tumour targeting, probably because F3-nanoworms were rapidly cleared from the blood (1 h) when compared to CREKA-nanoworms (circulation times >10 h). Using a longer PEG linker for the peptide attachment improved the targeting efficiency of CREKA-nanoworms. The targeting efficiency of both tumours was optimal for a nanoworm decorated with ≈60 CREKA peptides (designated as **NW-P175-C**), with a larger uptake in the case of HT1080 cells. In terms of biodistribution, most of the CREKA-nanoworms were found in the liver and spleen of the mice. Fluorescence images of tumours collected 24 h after injection of NW-P175-C revealed different localization of the nanomaterial, depending on the type of tumour: nanoworms were found in large blood vessels in MDA-MB-435 tumour cells, respectively in smaller vessels and tumour stroma in HT1080 cells. The authors postulated that the larger uptake observed in the case of HT1080 tumour can be attributed to a self-amplifying process induced by the binding of CREKA to clotted plasma proteins present in this type of tumour.

Ivanisevic and co-workers also showed that the introduction of RGD peptides as targeting moieties for the integrin cell-surface receptors of HT-29 human colon cancer cells led to an enhanced uptake of LBL-encapsulated DNA-templated Au–iron oxide nanoparticle chains.[63,64] The authors carried out a comparative *in vitro* study using the HT-29 cell line (human colon cancer cells) to evaluate the cytotoxicity and cellular uptake of nanoparticles alone, DNA-templated nanochains (1 : 1 DNA : NP ratio, where NP = Au, Fe_2O_3 or $CoFe_2O_4$) and LBL encapsulated DNA-templated nanochains functionalized with RGD on their outermost layer.[63] NPs alone induced mitochondrial damage, while DNA-templated nanochains showed no cytotoxic effect after 3 days of incubation. Moreover, the cellular uptake was significantly improved after LBL encapsulation

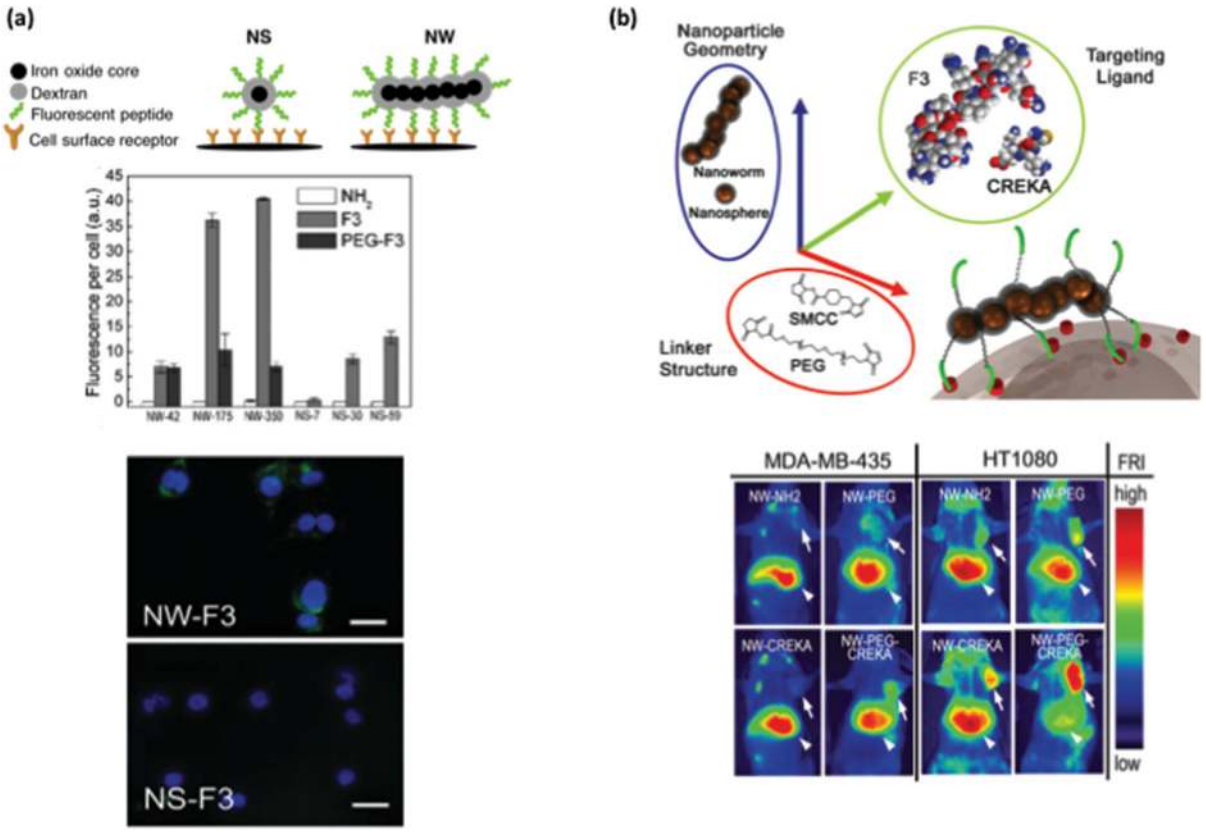

Fig. 11 (a) Internalization of spherical (NS) and high aspect ratio nanomaterials (nanoworms, NW) functionalized with F3 peptide by MDA-MB-435 cells. Top: elongated shape enables multivalent interactions between F3 peptides and cell-surface receptors. Middle: comparison of the internalization efficiency for different NS and NW formulations, obtained from fluorescence data. Bottom: fluorescence microscope images after 3 h of incubation of cells with NWs and NS modified with fluorescent FITC F3 peptides (green). Nuclei are stained with DAPI (blue). FITC: fluorescein isothiocyanate. Scale bars are 2 μm. Adapted from ref. 4 with permission from John Wiley & Sons. (b) Top: systematic surface engineering of nanomaterials for optimal *in vivo* tumour targeting. Three parameters – shape (blue oval), linker structure (red oval) and targeting peptide (green circle) – were optimized. Bottom: near infrared (NIR) fluorescence images of mice bearing MDA-MB-435 and HT1080 tumours obtained 24 h after injection with different NW formulations. Arrows and arrowheads indicate the tumours and the livers, respectively. Reprinted from ref. 5 with permission from John Wiley & Sons.

and introduction of RGD moieties, respectively. The cytotoxicity of the nanochains was assessed after the addition of each polymer layer without observing any significant decrease in cell viability. This is promising towards *in vivo* applications, as it suggests that degradation of the polymer coating would not affect cell viability.

In one of the most in-depth studies on the interaction between anisotropic magnetic nanoparticles and cells, Berret and co-workers showed that polymer-coated iron oxide nanowires without any targeting ligands on their surface could also be internalized by NIH/3T3 fibroblast cells after 24 h incubation.[76] Phase contrast microscopy revealed that the cells maintained their shape and adherence properties after 24 h incubation with nanowires and confirmed the presence of wires of different lengths (1–7 μm) inside cells (Fig. 12a–c). The authors further investigated the potential cytotoxicity of the nanowires and their spherical iron oxide building blocks in order to establish the influence of the nanomaterial's morphology on cell viability. Cell proliferation, mitochondrial activity measurement and reactive oxygen species (ROS) production revealed no short-term (<100 h) toxicity of either type of nanomaterial. Interestingly, TEM pictures acquired after a 24 h incubation with 15 μm nanowires showed that three types of nanomaterials could be observed inside intracellular compartments (surrounded by lipidic membranes, Fig. 12d, images 1 and 2) or in the cytosol (Fig. 12d, images 3 and 4), but not inside the nuclei: nanowires (entire or pieces), clusters of spherical nanoparticles and nanoparticles alone. This indicated that cells were able to degrade the initial nanowires and the degradation was attributed to the low pH inside lysosomal compartments and to the structure of the wires, which were composed of spherical nanoparticles held together by non-covalent interactions. In contrast, spherical nanoparticles were observed only inside membrane-bound compartments (Fig. 12d, images 5 and 6), suggesting a different cell internalization pathway depending on the shape of the nanomaterial. Immunofluorescence studies using lysosomal associated membrane protein 1 (LAMP1) markers confirmed the subcellular

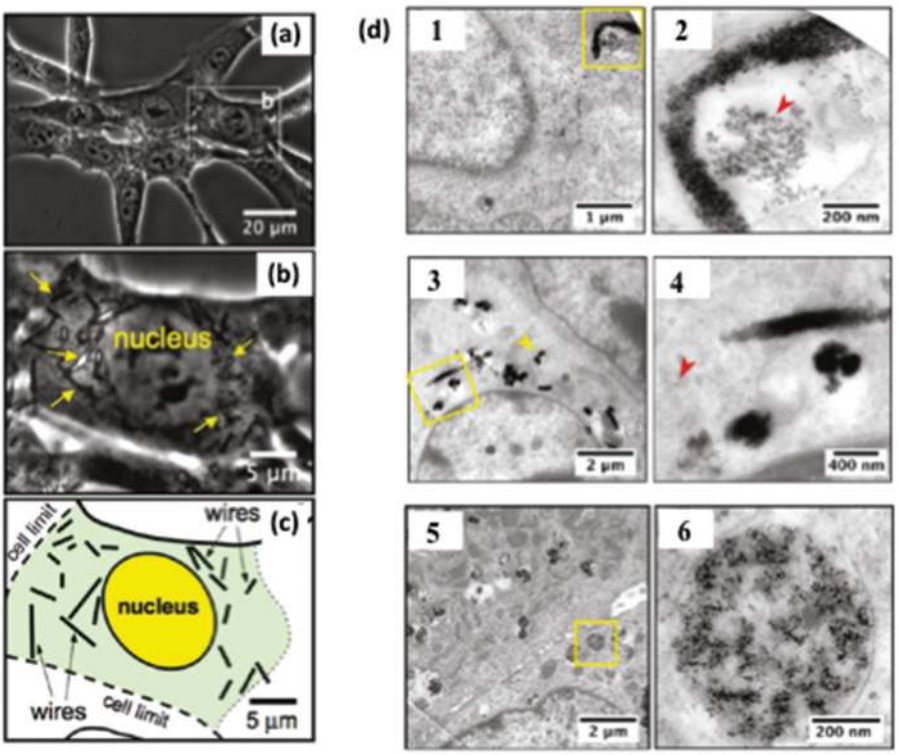

Fig. 12 Interaction of magnetic iron oxide nanowires with NIH/3T3 fibroblast cells. (a, b) Phase contrast microscopy images of cells incubated with 15 μm nanowires for 24 h. Yellow arrows in panel (b) indicate internalized wires of different lengths. (c) Schematic representation of the area depicted in image (b). (d) TEM images of internalized nanowires (images 1–4) and nanospheres (5 and 6) after 24 h. Images in the right column (2, 4 and 6) represent zoom-ins of the yellow rectangles in images 1, 3 and 5. Red arrows in images 1 and 4 indicate single nanoparticles resulted from degradation of nanowires. Top: nanowires inside intracellular compartments. Middle: nanowires dispersed in the cytosol. Bottom: spherical nanoparticles internalized in membrane-bound compartments. Reprinted with permission from ref. 76. Copyright 2011, American Chemical Society.

localization of the wires, although further studies are needed to unravel the internalization mechanism. The fact that the nanowires could be degraded inside cells without showing signs of cytotoxicity associated with other high aspect ratio nanomaterials[107] is a positive feature for possible bioapplications of such nanostructures.

Despite the increasing number of bioapplications of carbon nanotubes, there is still no consensus regarding their toxicity and adverse effects.[108] In addition, the potential cytotoxicity, biodistribution and elimination of hybrid CNT-magnetic nanomaterials would require a more in-depth investigation, as each individual component is expected to contribute to the overall toxicity of the material. In the reports published so far, hybrid CNT materials generally showed low toxicity on different cell lines and in one *in vivo* example, although cell viability was evaluated using different assays and the concentration range employed was not the same for all nanomaterials. Moreover, no detailed investigations on the fate of the hybrids after cell internalization have been carried out. Only one observation has been made in this regard by Bégin-Colin and co-workers, who pointed out that CNTs decorated with iron oxide nanoparticles were internalized by human prostate cancer cells (PC3) without signs of cytotoxicity or detachment of the iron oxide NPs from the CNT surface.[57] Therefore, more data are needed to obtain a global picture about the cytotoxicity and degradation mechanisms of this kind of high aspect ratio nanomaterial. Multiwalled carbon nanotubes–iron oxide (MWCNT-IO) hybrids reported by Yang and co-workers showed very low *in vitro* toxicity on MCF-7 (human breast adenocarcinoma) and L929 (mouse fibroblast) cell lines even at high concentrations (more than 80% cell viability after 24 h exposure to a concentration of 200 μg mL^{-1}).[54] These hybrids displayed a negligible haemolytic effect on human red blood cells, indicating their suitability for intravenous administration. The *in vivo* behaviour of the MWCNT–IO hybrids was investigated in mice after tail vein injection using histopathology and TEM microscopy to assess their biodistribution and inductively coupled plasma–atomic emission spectroscopy (ICP–AES) to determine the amount of Fe in organs. ICP results showed that the liver, lung and spleen were responsible for the uptake of the hybrids and no significant amounts were found in the heart and kidneys. At short times (4 h post-injection) the hybrids accumulated preferentially in the liver, while after prolonged exposure (8 h) they were found mainly in the spleen. Elimination studies revealed that the MWCNT–IO hybrids were mainly excreted in faeces, although a small amount of Fe was also found in urine up to 24 h after injection. Lu *et al.* evaluated the cellular uptake and *in vitro* cytotoxicity of

polymer-coated MWCNT–IO hybrids decorated with folic acid (FA) as the tumour targeting ligand.[55] Folate receptors are over-expressed on the surface of several types of cancer cells and folate-mediated targeting has been widely explored for diagnostics and therapeutic purposes.[109] FA–MWCNT–IO hybrids showed increased cellular uptake through receptor-mediated endocytosis in U87 (human glioblastoma cells); the uptake was significantly diminished when folate receptors on U87 cells were blocked with folic acid prior to incubation with the nanotubes. MTT cell viability assays carried out after two days of incubation with FA–MWCNT–IO hybrids confirmed their low toxicity on both cancer cells (U87) and normal cells (3T3 mouse fibroblasts) over a broad range of concentrations (0.001–1000 μg mL^{-1}). Similarly, Yin *et al.* reported improved cellular uptake of FA-conjugated magnetic CNT hybrids in HeLa (human cervical cancer) cells when compared to magnetic CNT hybrids lacking the folic acid targeting units.[56]

3.3 Magnetic separation and detection

Magnetic separation of cells and biomolecules is one of the most widespread applications of magnetic nanoparticles. The separation principle is generally based on recognition events between the cells or biomolecules of interest and magnetic nanoparticles with appropriate surface functionalization (*e.g.* antigen–antibody interactions or hybridization of complementary oligonucleotide strands).[13,110–112] Naturally, high aspect ratio magnetic nanomaterials were also explored for bioseparations, as their higher magnetic moment and ability to establish multivalent interactions with cells and biomolecules were thought to improve the yield of separation.

In one of the first examples of cell separation with anisotropic magnetic nanomaterials, Reich and co-workers showed that ferromagnetic Ni nanowires (35 μm length, 350 ± 40 nm diameter) performed better than commercially available superparamagnetic beads of comparable volume in the separation of mouse NIH-3T3 fibroblast cells.[40] The separation yield was higher by about a factor of two for the nanowires when compared to the beads (49 ± 3% *vs.* 19 ± 2%), which was attributed to the larger surface area and higher magnetic moment of the wires.

Mirkin and co-workers reported the use of triblock magnetic Au–Ni–Au nanorods for the separation of proteins and antibodies using specific Ni–histidine (His) and biotin–streptavidin binding strategies. In a first example, when the rods were exposed to a mixture of His-tagged and non-tagged proteins, the proteins bearing the histidine tag attached to the Ni segments of the rods and could be easily separated by applying a magnetic field (Fig. 13a, route 1).[44] Furthermore, using nanorods with the Au segments functionalized with nitrostreptavidin, the authors performed a simultaneous separation of a mixture of three proteins: a non-tagged protein, biotin-tagged BSA and His-tagged ubiquitin (Fig. 13b).[45] The separation efficiency of His-tagged and biotin-tagged proteins was higher than 90%, based on fluorescence measurements. Similarly, Au–Ni–Au nanorods functionalized with poly-His were employed to separate a mixture of fluorescently labelled anti-human immunoglobulin G (IgG) and anti-poly-His IgG (Fig. 13a, route 2).[44]

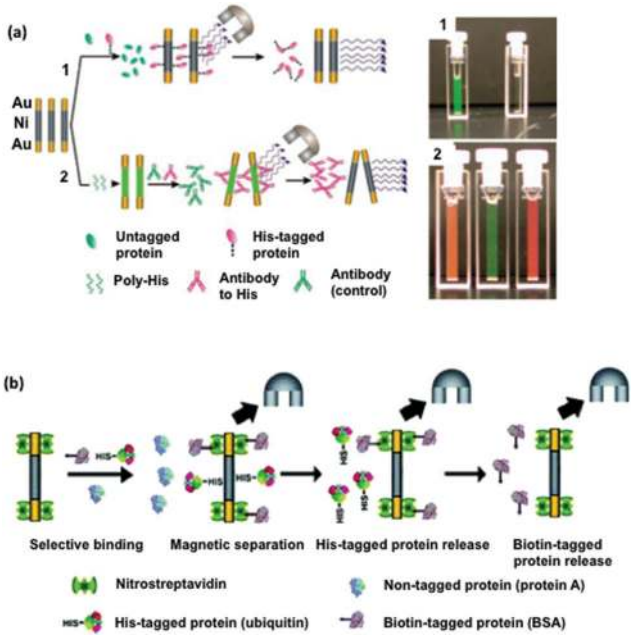

Fig. 13 Multisegment Au-magnetic nanorods for bioseparations. (a) Separation of proteins (route 1) and antibodies (route 2). Cuvettes in image 1 show a solution of fluorescein-tagged poly-histidine before and after magnetic separation. The orange cuvette in image 2 shows a mixture of His-tagged (red) and untagged (green) proteins. After exposure to Au–Ni–Au nanorods, the His-tagged protein is removed (thus the green colour observed in the middle cuvette containing the untagged protein). The red solution observed in the right hand-side cuvette is due to the release of the His-tagged protein. Reprinted from ref. 37 with permission from John Wiley and Sons. (2) Simultaneous separation of a tricomponent mixture of His-tagged, biotin-tagged and untagged proteins using Ni–His and biotin–streptavidin interactions. Reprinted with permission from ref. 45. Copyright 2006, American Chemical Society.

Son *et al.* employed magnetic nanotubes decorated with human IgG on their inner surface to selectively separate fluorescently labelled anti-human IgG from a solution containing also anti-bovine IgG.[51] Fluorescence spectra revealed that 84% of the anti-human IgG was separated by IgG-nanotubes, while in a control experiment using magnetic nanotubes functionalized with bovine serum albumin (BSA), the nonspecific separation yield was significantly lower (9%).

Dextran-coated iron oxide (DION) superparamagnetic nanorods conjugated with anti-MAP antibodies (MAP = *Mycobacterium avium* spp. *paratuberculosis*) were efficiently used as magnetic sensors for the detection of bacteria.[27] Due to their magnetic and shape anisotropy, the rods were superior to similar spherical nanoparticles,[113] both in terms of kinetics and limit of detection. The improved limit of detection observed was attributed to the possibility of introducing a high number of antibodies on the surface of the nanorods when compared to the spherical nanoparticles. Prina-Mello *et al.* also took advantage of the high aspect ratio of fluorescent

magnetic nanowires to maximise the efficiency of nanowire-cell binding for immunodetection applications using flow cytometry.[50] Multiple copies of primary IgG antibody R-phycoerythrin (R-PE) conjugated to secondary human CD54 (intracellular adhesion molecule 1, ICAM-1) functionalized with fluorescein were introduced on the surface of the wires, resulting in a uniform coverage. Once again, nanowires outperformed their spherical analogues for the detection of human acute monocytic leukemia cells (THP-1) binding to ICAM-1. Although the percentage of cells binding to nanospheres was higher than that binding to wires (62% *vs.* 17%), the nanowires were used at a much lower concentration (1.00×10^7 mg mL^{-1}) than the spherical nanoparticles (6.50×10^8 mg mL^{-1}). Moreover, the nanowires did not show any tendency to form clusters in solution, as opposed to spherical nanoparticles, which represents an additional advantage for multiplexed flow cytometry applications.

3.4 Targeted drug delivery

The main advantages of targeted delivery of therapeutics over topical application are a better efficacy because of the high local concentration of drug and reduced adverse effects due to a very low systemic exposure. Cancer is particularly attractive for targeted delivery for two reasons. On the one hand, tumour cells and vasculature present characteristics that distinguish them from healthy cells and blood vessels, expressing specific molecules that can be used for selective recognition by delivery vehicles (see the review by Ruoslahti *et al.*[114]). On the other hand, targeted delivery of anticancer compounds would reduce the exposure of healthy tissues to aggressive chemotherapeutics, while ensuring a high local concentration of drug, thus alleviating important problems of traditional cancer therapy methods.[12]

Nanomaterials present unique opportunities for the targeted delivery and controlled release of the drug. In particular, engineered magnetic nanoparticles can perform cooperative targeting, diagnostic (MRI) and therapeutic (drug release and/or magnetic hyperthermia) functions and, due to their magnetic properties, their targeting can be improved by magnetic guidance. Nevertheless, designing nanoparticles for drug delivery is a challenging task. As indicated in section 3, nanomaterials for biomedical applications must be robust enough to overcome a series of biological barriers and reach their target in a pharmaceutically relevant concentration and without loss or alteration of their function. In addition, the distinct features of tumour cells and vasculature, although providing specific markers for targeting, make difficult the access of nanomaterials to the majority of cancer cells.

High aspect ratio nanomaterials can be decorated with multiple recognition elements to improve their tumour targeting by establishing multivalent interactions with markers present on the surface of cancer cells. Sailor and Ruoslahti extensively exploited this feature to develop more efficient targeting and delivery systems based on anisotropic nanomaterials. Their initial work using superparamagnetic iron oxide nanoworms (NWs) focused on the optimization of the tumour targeting efficiency by tuning the surface functionalization of the nanomaterial (see also section 3.2).[4,5] Different peptides were explored as targeting elements, based on the fact that many peptides are known to have cell- and tumour-penetrating properties[115] or can act as tumour vasculature markers.[116–118] Multifunctional nanoworms decorated with a chimeric peptide composed of a tumour vasculature targeting element (CGKRK) and a therapeutic agent ($_D$[KLAKLAK]$_2$, known to initiate apoptosis by disrupting the membrane of mitochondria) were explored as potential therapy for glioblastoma.[119] The system was tested in murine models for two types of brain tumours and succeeded in eliminating most lentiviral-induced brain tumours in mice and increasing the survival period of mice with more aggressive U87 glioblastoma. The exceptional effectiveness of this therapeutic nanomaterial is due to several key design elements. On the one hand, the targeting component CGKRK not only targeted the tumour vasculature, but also mitochondria, ensuring the subcellular targeted delivery of the therapeutic payload $_D$[KLAKLAK]$_2$. Nanoworms bearing only the proapoptotic peptide (without the homing peptide) showed no targeted delivery and were not effective against brain tumours. On the other hand, the elongated geometry of the iron oxide nanoworms enhanced the cell internalization due to multivalent interactions (*vide supra*). Targeted subcellular delivery and multivalent presentation on elongated nanocarriers made possible the lowering of the necessary dose of $_D$[KLAKLAK]$_2$ by 100-fold, which reduced the adverse effects associated with the high toxicity of the peptide at therapeutic doses. Co-administration of the CGKRK$_D$[KLAKLAK]$_2$-NWs together with the tumour-penetrating peptide iRGD further improved the efficacy of the treatment by allowing the nanoparticles to reach the tumour cells in addition to tumour blood vessels. Finally, the magnetic properties of the nanoworms were used to further confirm their localization inside brain tumours on magnetic resonance images.

The nanoworms were further employed as part of cooperative nanomaterial systems for amplified tumour targeting and therapy purposes.[120] Au nanorods (NRs) that passively accumulate in tumours were used to induce photothermal activation of the tumour microenvironment by absorption of near-infrared (NIR) radiation. This in turn amplified *in vitro* tumour targeting by magnetic nanoworms (NWs) decorated with LyP-1, a cyclic nine amino acid peptide that selectively binds p32 receptors overexpressed on the surface of certain types of cancer cells upon exposure to thermal stress. Mice with MDA-MB-435 human carcinoma tumours and C8161 human melanoma (whose level of p32 receptors is much lower than that for MDA-MB-435) were injected with control NWs and LyP1NWs to examine the possibility of selective *in vivo* tumour homing. Increased cellular uptake of LyP1NWs was observed in MDA-MB-435 tumours upon heating to 45 °C in a water bath for 30 min when compared to unheated tumours. Conversely, the ability of the nanoworms to target heated and non-heated C8161 tumours was not significantly different. Similarly, the authors demonstrated that *in vivo* MDA-MB-435 tumour targeting of therapeutic nanoparticles (LyP1 liposomes

carrying doxorubicin) was significantly enhanced by NR-mediated photothermal heating. Moreover, although photothermal therapy alone could not reduce tumour volumes, its combination with therapeutic nanoparticles revealed substantial tumour regression and even eradication. The authors explained the success of their cooperative therapy by the fact that cells exposed to NR-heating were more sensitive to subsequent exposure to chemotherapy.

Using an ingenious design inspired by communication in biological systems, Bhatia and co-workers developed a two-component nanosystem to amplify *in vivo* targeting. The system consists of a "signalling" module (nanoparticles or proteins) that targets tumours and then transmits their location to a "receiving" module (circulating nanoparticles carrying diagnostic or therapeutic payloads) through the activation of a biological cascade (Fig. 14a).[121] The authors chose the coagulation process as a tool for transmitting communication between signalling (Au nanorods or tumour-targeted tissue factor tTF-RGD) and receiving (multimodal magnetic-fluorescent iron oxide nanoworms or doxorubicin-loaded liposomes) components using two molecular pathways: activity of coagulation transglutaminase factor XIII (FXIII) or targeting of polymerized fibrin. Signalling modules induced coagulation in tumours through photothermal conversion of NIR radiation (Au NRs) or by binding to angiogenic $\alpha_v\beta_3$ receptors in tumour vasculature (tTF-RGD). Receiving nanoparticles were engineered to target coagulation regions in tumours and deliver imaging or therapeutic agents. Accordingly, nanoworms and liposomes were functionalized with factor XIII substrates or fibrin-binding peptides to address both molecular pathways in the coagulation cascade. The capacity of the integrated system to communicate and amplify *in vivo* tumour targeting and drug delivery was evaluated in mice bearing MDA-MB-435 tumours. FXIII-NWs showed more than one order of magnitude increase in accumulation in tumours following NR administration and thermal NIR irradiation when compared to unirradiated tumours. Similarly, tTF-RGD signalling modules co-injected with the nanoworms amplified their tumour targeting by several-fold over non-communicating systems. It is noteworthy that this strategy significantly improved the delivery of therapeutic nanoparticles to tumours, with a 40-fold increase in the accumulation of doxorubicin-loaded liposomes compared to liposomes alone.

A similar amplification system based on communication between signalling and receiving nanoparticles was further designed using changes in the tumour microenvironment to mediate increased targeting.[122] The system was composed of signalling Au nanorods and responding magnetic nanoworms (Fig. 14b). Upon NIR irradiation, Au NRs induced denaturation of Type I collagen present in the extracellular matrix of tumour cells, thus altering its tri-helical tertiary structure and exposing cryptic epitopes to fibronectin-functionalized magnetic nanoworms (FnF-NWs) for selective targeting of denatured collagen. This cooperative system resulted in a six-fold enhancement in

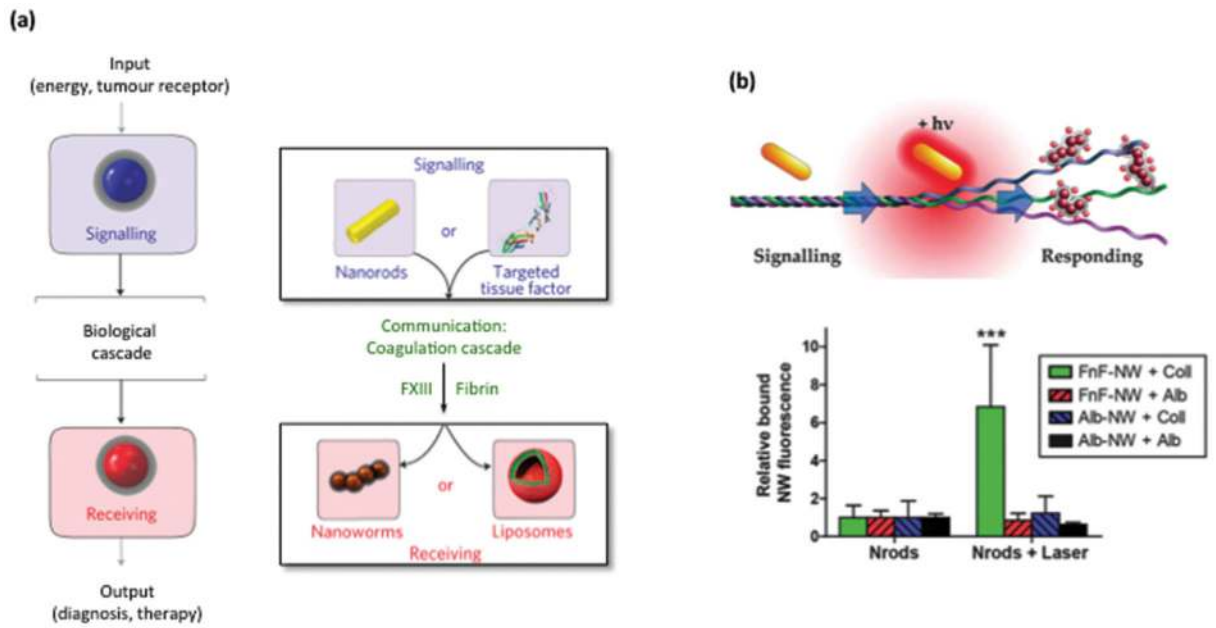

Fig. 14 Amplification of tumour targeting with communicating nanoparticles. (a) Schematic representation of the communication system involving signalling modules (Au nanorods or engineered proteins) that use a biological cascade (coagulation) to transmit the information to receiving components (inorganic magnetic nanoworms or organic drug-loaded liposomes). Adapted from ref. 121 by permission from Macmillan Publishers Ltd (*Nat. Mater.*, 2011, **10**, 545), copyright 2011. (b) Photothermal denaturation of collagen exposes cryptic binding sites for recognition by fibronectin-conjugated magnetic nanoworms, resulting in enhanced tumour targeting. Reprinted from ref. 122 with permission from The Royal Society of Chemistry.

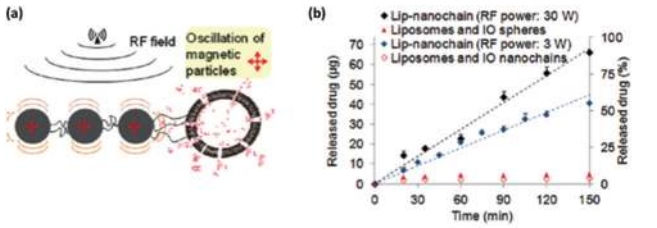

Fig. 15 (a) Radio-frequency induced tuneable drug release from magnetic nanochains exploiting defects in the liposomal membrane induced by mechanical vibrations of the magnetic nanoparticle chain. (b) *In vitro* triggered release of doxorubicin from different nanocarriers using an RF field at 10 kHz. Reprinted with permission from ref. 90. Copyright 2011, American Chemical Society.

binding of the FnF-NWs over non-heated controls or experiments using control substrates (albumin) and control targeting moieties on the receiving nanoworms (albumin-NWs). Although the ability of the system to induce nanoparticle amplification was tested only *in vitro*, it can be anticipated that this approach would be successful *in vivo*, as local hyperthermia induced by the Au NRs would trigger changes in the tumour vasculature, making possible the recruitment of the responding nanoparticles. Another attractive feature of this approach is the fact that it displays binding sites that are not normally accessible under physiological conditions, while other typical receptor-mediated nanoparticle delivery systems require upregulation of cell-surface receptors.[120]

Peiris *et al.* developed a multicomponent nanomaterial for enhanced delivery of chemotherapeutics consisting of three iron oxide nanospheres and one doxorubicin-loaded liposome covalently assembled in a nanochain[89] with a length of 100 nm.[90] The magnetic nature of the nanoparticles was used to trigger the controlled release of the drug from the liposomes upon exposure to a radiofrequency (RF) field (Fig. 15). Mechanical vibrations induced by oscillations of the magnetic nanoparticles were thought to be responsible for the controlled release of the drug by causing defects in the liposome membrane. This release mechanism was confirmed by the fact that the release was concentration-independent, but significantly affected by the distance from the RF coil. The nanochains outperformed 100 nm spherical doxorubicin-loaded liposomes both in terms of blood circulation time (26 h half-life compared to 18 h for 100 nm liposomes) and intratumoral uptake in mice bearing 13762 MAT BIII mammary adenocarcinoma. Application of an RF field 24 h after the intravenous administration of the nanochains resulted in significant inhibition of tumour growth, as opposed to conventional doxorubicin or liposome-doxorubicin treatment.

3.5 Magnetic resonance imaging (MRI)

Magnetic resonance imaging (MRI) is a non-invasive imaging technique widely employed for diagnostic purposes based on high-resolution anatomical information, resulting from the different magnetic surroundings of the protons in water molecules in tissues. Magnetic nanoparticles are commonly used as contrast enhancement agents for MRI due to their ability to shorten the transverse relaxation times (T_2 and T_2*) of water protons in their vicinity.[9,10,16] This results in the darkening of the tissue containing magnetic nanoparticles, therefore the name of "negative" contrast agents (as opposed to rare earth metal complexes that are used as "positive" contrast agents by reducing the longitudinal relaxation time T_1). Some of the high aspect ratio magnetic nanomaterials described in the literature have shown great potential as MRI contrast agents, in some instances surpassing their spherical counterparts. Nevertheless, most examples report data obtained in solution or phantom media and more *in vitro* and *in vivo* studies are needed in order to have a clearer global picture of the real potential of such nanomaterials.

The efficiency of a contrast agent is typically measured in terms of longitudinal and transverse relaxivities ($R_1 = 1/T_1$ and $R_2 = 1/T_2$), defined as the increase of the relaxation rate of water produced by 1 mmol L^{-1} of the active ion (Gd, Fe, *etc.*).[10] Usually, R is plotted against Fe concentration and the slope of the curve yields the concentration-independent relaxivity (r_1, r_2). Gun'ko and co-workers investigated the nuclear magnetic resonance dispersion (NMRD) profile of chains of iron oxide nanoparticles assembled on single-stranded and double-stranded DNA,[59] respectively on PSSS.[17] DNA composites showed unusually high r_1 relaxivities at low magnetic field, especially in the case of the single-stranded assembly. The authors reasoned that the better ordering on denatured DNA templates, resulting in a higher concentration of magnetic nanoparticles, might be the cause of the unexpected high r_1 value. NMRD curves of PSSS assemblies of magnetic nanoparticles showed higher values for the r_2 relaxivity when compared to r_1 at different magnetic fields and temperatures. The PSSS composites were evaluated for *in vivo* MR imaging in rats. Although the authors did not report extensive toxicity and biodistribution data, they mention no signs of adverse reactions after 24 h of injection. MR images obtained at 7 T using Echo Planar Imaging (EPI) and Fast Low Angle Shot (FLASH) sequences before and after injection of the nanomaterial into the tail vein of rats showed that this reached the brain after approximately 12 s (Fig. 16a), and the occlusion of the sinus superior sagittalis (SSS) vein could be clearly identified on the FLASH image. Based on these initial observations, the authors acknowledged the potential of high aspect ratio magnetic nanoparticles for *in vivo* MRI and attributed their easy circulation through the blood vessels to their elongated shape. However, no comparison with the individual spherical building blocks was carried out in this regard.

Superparamagnetic iron oxide nanoworms described by Sailor and co-workers showed better contrast and higher r_2 relaxivities at 4.7 T in solution (116 mM^{-1} s^{-1}) when compared to similar spherical nanoparticles (70 mM^{-1} s^{-1}) and commercially available Feridex (95 mM^{-1} s^{-1}).[4] The initial explanation of the authors attributed the result to the linear aggregation of spherical iron oxide nanoparticles, which might result in enhanced spin–spin relaxation of water molecules. In a more

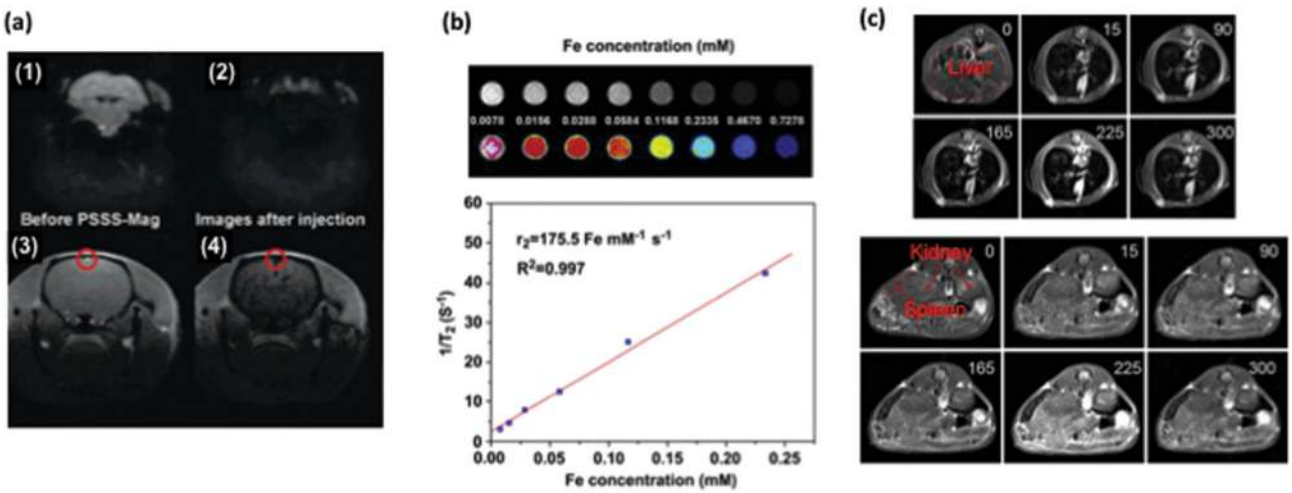

Fig. 16 (a) *In vivo* evaluation of magnetic nanowires as MRI contrast agents. EPI (1 and 2) and FLASH (3 and 4) scans of mouse brain before and after injection of the magnetic nanomaterial (see text for abbreviation of the MRI pulse sequences). Reprinted with permission from ref. 17. Copyright 2008, American Chemical Society. (b) MWCNT–IO hybrids as contrast agents for MRI. T_2-Weighted MR images of water suspensions of MWCNT–IO hybrids with different concentrations (top) and plot of the relaxation time against Fe concentration (bottom). (c) *In vivo* T_2-weighted images of liver (top), spleen and kidneys (bottom) at different time points after intravenous administration of the MWCNT–IO hybrids. Reprinted from ref. 54, H. Wu *et al.*, The behavior after intravenous injection in mice of multiwalled carbon nanotube/Fe_3O_4 hybrid MRI contrast agents, *Biomaterials*, **32**, 4867–4876, Copyright 2011, with permission from Elsevier.

elaborate study, the authors further investigated the magnetic properties of the nanoworms and obtained the NMRD profile at different temperatures.[18] A linear increase of the r_2 relaxivity with the magnetic field was observed and the obtained values were consistent with numerical simulations conducted both on individual spherical nanoparticles and linear clusters.[18,123] Similarly, Peiris *et al.* reported a 2.5-fold increase in the transverse relaxivity of nanochains assembled by covalent linking of three spherical nanoparticles when compared to individual nanoparticles.[89] This linear chain showed an r_2 value of 101 mM^{-1} s^{-1} at 1.4 T and 40 °C, superior to that reported by Sailor and co-workers for the nanoworms[18] (64.8 mM^{-1} s^{-1} at the same magnetic field and 37 °C).

Wu *et al.* reported a comprehensive *in vitro* and *in vivo* study of MWCNT–IO hybrids as potential MRI contrast agents.[54] Water suspensions of MWCNT hybrids with different Fe concentration were imaged at 3.0 T in a clinical MRI scanner at room temperature, showing a decrease in signal intensity with increasing concentration of iron (Fig. 16b). Images of MCF-7 cells incubated with different concentrations of MWCNT–IO hybrids also revealed a significant negative contrast enhancement. The decrease in the MRI signal was higher at higher concentrations of contrast agent, due to the enhanced cellular uptake. Finally, the authors explored the potential of the MWCNT–IO hybrids for *in vivo* imaging. T_2-Weighted MR images were acquired before and at different time points after the injection of the hybrids in the tail vein of mice at a dose of 2.5 mg Fe per kg body weight. The significant decrease in the signal intensities of liver and spleen revealed that these two organs were responsible for the relatively quick uptake (15 min) of the MWCNT–IO hybrids (Fig. 16c). Jia and co-workers investigated water-dispersible carbon nanotubes decorated with iron oxide nanoparticles as novel contrast agents for MRI.[56] These CNT hybrids showed promising results both in solution and *in vitro*. However, the authors reported the efficiency of their contrast agent in terms of effective transverse relaxivity (r_2* = 263 mM^{-1} s^{-1} at 3.0 T; the effective transverse relaxation time T_2* takes into account magnetic field inhomogeneities and is always smaller than T_2), therefore a comparison with similar carbon nanotube-based contrast agents cannot be made. To evaluate the potential of the nanotubes for MRI targeted cancer detection, HeLa cells were incubated with two types of magnetic CNTs, one functionalized with folic acid as the targeting unit and one without and MRI images were acquired after 6 h (see also section 3.2). Cells incubated with the nanotubes functionalized with folic acid showed lower T_2* relaxation times and higher negative contrast than those incubated with the nanomaterial lacking the targeting moiety. This observation confirms the importance of ensuring the cellular uptake of a contrast agent through its appropriate surface functionalization. Lamanna *et al.* reported that carbon nanotubes decorated with iron oxide nanoparticles using the ligand exchange approach (see page 6) showed a slightly lower longitudinal relaxivity (13 mM^{-1} s^{-1}) than the corresponding spherical IO nanoparticles (19 mM^{-1} s^{-1}). This could be explained by the fact that the proton accessibility to magnetic centres is impaired by the aggregation of the NPs on the surface of the CNTs. On the other hand, the transverse relaxivity showed a slight increase (from 88 mM^{-1} s^{-1} for the NPs alone to 103 mM^{-1} s^{-1} for the nanotube hybrids), which was attributed by the authors to the larger local magnetic field produced by the assembly of the

NPs. Cells incubated with the CNT–NP hybrids could be detected by MRI in agarose gels as hypointense areas whose density was proportional to the number of cells seeded in the gels. This observation suggests that such CNT–NP nanoconstructs have potential as MRI contrast agents for cell tracking.

The group of Ivanisevic devoted much effort to the development of efficient MRI contrast agents based on DNA-templated high aspect ratio magnetic nanomaterials.[60–65] The authors investigated different chain compositions (Au, Fe_2O_3 or $CoFe_2O_4$ single- and multicomponent chains), DNA : nanoparticle (NP) ratios, as well as LBL-encapsulated *vs.* non-encapsulated DNA-chains. DNA–NP chains shortened the transverse relaxation times when compared to individual nanoparticles, with the exception of single-component Au NP chains, in which no difference could be appreciated between the chains and the Au NPs. Although for DNA : NP ratios of 1 : 5 and 1 : 10 the observed shortening in T_2 was more pronounced than for the 1 : 1 ratio, these chains had poorer colloidal stability and were not further investigated. The proposed relaxation mechanism suggests that the shortening of T_2 relaxation times was due an increase in the magnetization upon magnetic nanoparticle alignment on the DNA template as well as to possible inter-segment interactions that could also alter the overall magnetization of the system (Fig. 17a).[65] Optimised single- and multicomponent chains were then subjected to an exhaustive MRI study in cell culture phantoms, in order to mimic *in vivo* environments (Fig. 17b).[64] Table 2 summarizes the transverse relaxivities obtained in a clinical 3 T MRI scanner for several DNA–NP constructs both before and after LBL encapsulation. Studies were conducted in Matrigel (a gelatinous protein mixture resembling the extracellular environment) and in 3D cell cultures in Matrigel. These experiments can provide a quick and inexpensive assessment of the efficiency of MRI contrast agents prior to *in vivo* studies. In Matrigel, single-component magnetic chains, as well as Au-magnetic multicomponent chains, showed a remarkable increase in r_2 values compared to dispersed nanoparticles (up to 12-fold in the case of Au–Fe_2O_3 chains). However, in 3D cell cultures there were no significant differences between NPs and NP chains, and the measured values were generally lower than those measured in Matrigel alone. Previous observations on 2D cell cultures indicated that chains and nanoparticles were both internalized by cells in a similar fashion and accumulated into vesicles, independent of their shape.[63] The authors postulated that this agglomeration was responsible for the

Table 2 Transverse relaxivities for single-component and multicomponent nanoparticle chains in Matrigel and in 3D cell cultures compared to dispersed nanoparticles. Adapted with permission from ref. 64. Copyright 2011, American Chemical Society

		r_2 (mM^{-1} s^{-1})		
	Nanomaterial	Dispersed NPs	NP chains	Encapsulated NP chains
Matrigel	**Single component**			
	Au	10.1 ± 5.8	10.0 ± 6.0	—
	Fe_2O_3	12.2 ± 0.3	78.6 ± 5.8	—
	$CoFe_2O_4$	21.7 ± 15.6	114.0 ± 34.0	—
	Multicomponent			
	Au–Fe_2O_3	9.7 ± 6.0	120.4 ± 12.6	75.4 ± 8.1
	Au–$CoFe_2O_4$	21.3 ± 1.5	89.5 ± 11.0	55.5 ± 16.6
Cells in Matrigel	**Single component**			
	Au	5.0 ± 1.2	2.5 ± 2.0	—
	Fe_2O_3	4.6 ± 3.4	12.3 ± 8.0	—
	$CoFe_2O_4$	8.0 ± 4.7	11.8 ± 7.4	—
	Multicomponent			
	Au–Fe_2O_3	7.2 ± 4.0	8.8 ± 3.2	11.8 ± 4.8
	Au–$CoFe_2O_4$	6.0 ± 4.0	13.3 ± 6.4	6.8 ± 1.3

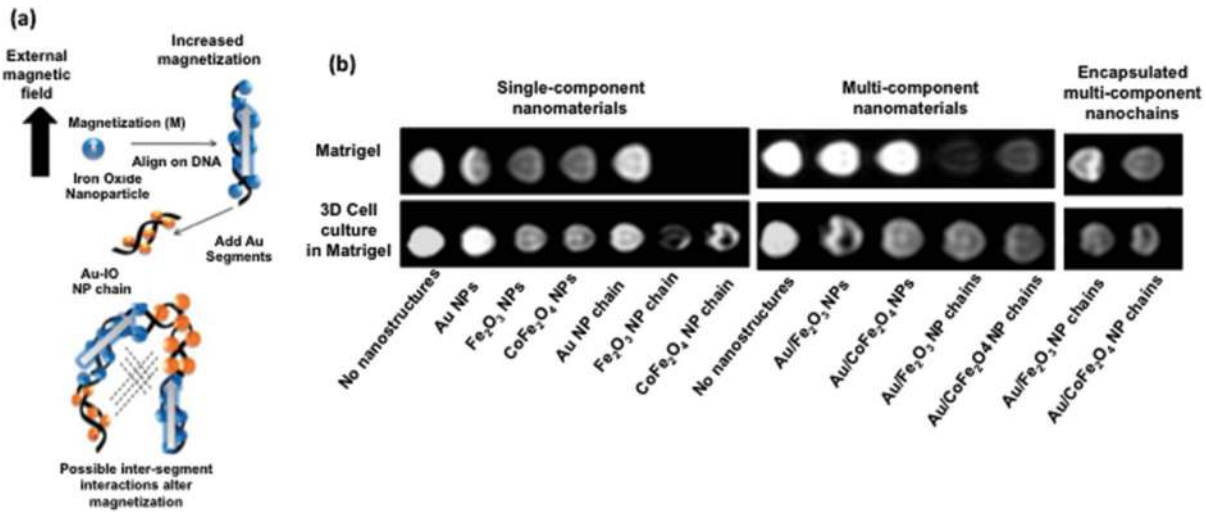

Fig. 17 (a) Proposed mechanism for the relaxation induced by DNA-Au-magnetic nanoparticle chains. Reprinted from ref. 65 with permission from The Royal Society of Chemistry. (b) T_2-Weighted MR images showing contrast in Matrigel and 3D cell culture scaffolds using DNA-templated nanoparticle chains. For a depiction of the chain structures, see Fig. 6. Reprinted with permission from ref. 64. Copyright 2011, American Chemical Society.

similar transverse relaxivity values observed for NPs and NP chains in 3D cell cultures. Upon LBL encapsulation, a decrease in the transverse relaxivity was observed in Matrigel phantoms. However, in 3D cell culture phantoms no significant differences were found, as in this case MRI contrast would be governed by the cellular uptake, which improved significantly upon encapsulation. To sum up, these studies revealed that in phantoms the MRI contrast was clearly better when using high aspect ratio nanomaterials. Conversely, in cell cultures the contrast was governed by the cell uptake efficiency rather than by the shape of the nanomaterial.

4. Concluding remarks and perspectives

Although much less explored than spherical nanoparticles, anisotropic magnetic nanomaterials possess attractive qualities for biomedical applications. In this work we present an overview of the synthesis of high aspect ratio magnetic nanomaterials and give examples of their applications in different fields: magnetic separation and detection, targeted delivery and magnetic resonance imaging, highlighting those examples in which anisotropic nanomaterial surpassed their spherical counterparts.

However, despite the advances in the field and the clear promise of these nanomaterials, research on this topic is still in its infancy and several challenges need to be addressed. In our opinion, the following two aspects deserve special attention and a more thorough investigation in the future:

(1) *Synthesis optimization.* Despite obvious progress and some very elegant approaches reported, there is a need to optimize the synthesis of anisotropic magnetic nanomaterials. Ideally, cheap, general and high-throughput synthetic procedures allowing for reproducible, large-scale synthesis of high aspect ratio magnetic nanomaterials with good control over their shape and magnetic properties are desirable. Probably the most successful routes will focus on electrodeposition in porous templates and assembly from individual building blocks. The use of templates permits an excellent control over the shape of the resulting anisotropic nanomaterials and offers the possibility of constructing multi-segmented nanostructures. Creating linear assemblies from spherical magnetic nanoparticles enables a good control of the length and the magnetic properties of the resulting linear assembly (usually, the resulting high aspect ratio preserves the magnetic properties of the initial individual components). Moreover, this method would capitalize on some already optimized methods for the synthesis of spherical magnetic nanoparticles. Last but not least, research in the field of high aspect ratio magnetic nanoparticles would definitely benefit from more in-depth mechanistic studies (including theoretical calculations) to unravel the mechanism of formation of such nanostructures.

(2) *Investigation of the cytotoxicity and interaction with biological entities.* The development of novel nanomaterials inevitably raises questions related to their potential toxicity. As high aspect ratio nanomaterials interact with cells in significantly different ways when compared to spherical nanoparticles, it is essential to assess their internalization pathways, effect on cell viability and degradation routes. Some detailed studies in this direction have already been reported; however, more research needs to be done in order to gain a better understanding of the cytotoxicity of anisotropic nanomaterials. A very important aspect is to relate the toxic effects to the size and concentration of high aspect ratio nanomaterials. For instance, some studies seem to indicate that short Ni nanowires are less toxic than longer ones, but at this point we are far from able to generalize their behaviour. Systematic studies using different cell lines and types of assays would shed more light on the interaction of anisotropic magnetic nanomaterials with cells and would provide useful information prior to *in vivo* studies.

The superiority of anisotropic magnetic nanomaterials over their spherical analogues has been demonstrated in some of the examples discussed in this review. Especially in the case of targeted drug delivery and magnetic resonance imaging applications, there is clear evidence to relate improved cell targeting and better magnetic properties to the shape and magnetic anisotropy. Therefore, we are confident that the field will continue its growth in the coming decades and the quest for new, exciting applications of high aspect ratio nanomaterials in biomedicine will follow. In particular, we believe that three areas could capitalize on the unique properties of these high aspect ratio nanostructures. Firstly, they could become valuable MRI diagnostic tools for the early detection of tumours and other disorders, due to their good magnetic sensitivity. Secondly, although barely investigated to date, the use of anisotropic magnetic nanomaterials for hyperthermia therapy of cancer is definitely worth exploring, as it could lead to better therapeutic solutions. Thirdly, anisotropic magnetic nanomaterials could improve the efficacy of existing targeted drug delivery systems based on nanotechnology approaches.

Acknowledgements

This work was supported by ERC-Starting Grant 239931-NANOPUZZLE, Shanghai 1000 People Plan and Fondo Social Europeo (FSE, Gobierno de Aragón). R. M. F. acknowledges financial support from ARAID and the University of Zaragoza.

Notes and references

1 M. Prato, R. Singh, D. Pantarotto, L. Lacerda, G. Pastorin, A. Bianco and K. Kostarelos, *Proc. Natl. Acad. Sci. U. S. A.*, 2006, **103**, 3357.
2 Z. Liu, W. Cai, L. He, N. Nakayama, K. Chen, X. Sun, X. Chen and H. Dai, *Nat. Nanotechnol.*, 2007, **2**, 47.
3 Y. Geng, P. Dalhaimer, S. Cai, R. Tsai, M. Tewari, T. Minko and D. E. Discher, *Nat. Nanotechnol.*, 2007, **2**, 249.

4 J.-H. Park, G. von Maltzahn, L. Zhang, M. P. Schwartz, E. Ruoslahti, S. N. Bhatia and M. J. Sailor, *Adv. Mater.*, 2008, **20**, 1630.

5 J. Park, G. Von Maltzahn, L. Zhang, A. M. Derfus, D. Simberg, T. J. Harris, E. Ruoslahti, S. N. Bhatia and M. J. Sailor, *Small*, 2009, **5**, 694.

6 O. Veiseh, J. W. Gunn and M. Zhang, *Adv. Drug Delivery Rev.*, 2010, **62**, 284.

7 M. Mammen, S.-K. Choi and G. M. Whitesides, *Angew. Chem., Int. Ed.*, 1998, **37**, 2754.

8 L. A. Bauer, N. S. Birenbaum and G. J. Meyer, *J. Mater. Chem.*, 2004, **14**, 517.

9 Q. A. Pankhurst, J. Connolly, S. K. Jones and J. Dobson, *J. Phys. D: Appl. Phys.*, 2003, **167**, R167.

10 S. Laurent, D. Forge, M. Port, A. Roch, C. Robic, L. Vander Elst and R. N. Muller, *Chem. Rev.*, 2008, **108**, 2064.

11 Q. A. Pankhurst, N. K. T. Thanh, S. K. Jones and J. Dobson, *J. Phys. D: Appl. Phys.*, 2009, **224001**, 1.

12 M. Colombo, S. Carregal-Romero, M. F. Casula, L. Gutiérrez, M. P. Morales, I. B. Böhm, J. T. Heverhagen, D. Prosperi and W. J. Parak, *Chem. Soc. Rev.*, 2012, **41**, 4306.

13 Y. Pan, X. Du, F. Zhao and B. Xu, *Chem. Soc. Rev.*, 2012, **41**, 2912.

14 J. Gallo, N. J. Long and E. O. Aboagye, *Chem. Soc. Rev.*, 2013, **42**, 7816.

15 D. Issadore, Y. I. Park, H. Shao, C. Min, K. Lee, M. Liong, R. Weissleder and H. Lee, *Lab Chip*, 2014, **14**, 2385.

16 L. H. Reddy, J. L. Arias, J. Nicolas and P. Couvreur, *Chem. Rev.*, 2012, **112**, 5818.

17 S. A. Corr, S. J. Byrne, R. Tekoriute, C. J. Meledandri, D. F. Brougham, M. Lynch, C. Kerskens, L. O'Dwyer and Y. K. Gun'ko, *J. Am. Chem. Soc.*, 2008, **130**, 4214.

18 Y. Gossuin, S. Disch, Q. L. Vuong, P. Gillis, R. P. Hermann, J.-H. Park and M. J. Sailor, *Contrast Media Mol. Imaging*, 2010, **5**, 318.

19 B. I. Kharisov, O. V. Kharissova and M. Jose-Yacaman, *Ind. Eng. Chem. Res.*, 2010, **49**, 8289.

20 C. J. Murphy and N. R. Jana, *Adv. Mater.*, 2002, **14**, 80.

21 *Nanomedicine - Design and applications of magnetic nanomaterials, nanosensors and nanosystems*, ed. V. K. Varadan, L. Chen and J. Xie, John Wiley & Sons, Ltd, 2008.

22 B. Y. Xia, P. Yang, Y. Sun, Y. Wu, B. Mayers, B. Gates, Y. Yin, F. Kim and H. Yan, *Adv. Mater.*, 2003, **15**, 353–389.

23 W. Wu, X. Xiao, S. Zhang, J. Zhou, L. Fan, F. Ren and C. Jiang, *J. Phys. Chem. C*, 2010, **114**, 16092.

24 T. P. Almeida, M. Fay, Y. Zhu and P. D. Brown, *J. Phys. Chem. C*, 2009, **113**, 18689.

25 I. Milosevic, H. Jouni, C. David, F. Warmont, D. Bonnin and L. Motte, *J. Phys. Chem. C*, 2011, **115**, 18999.

26 A. F. Rebolledo, O. Bomatí-Miguel, J. F. Marco and P. Tartaj, *Adv. Mater.*, 2008, **20**, 1760.

27 S. Nath, C. Kaittanis, V. Ramachandran, N. S. Dalal and J. M. Perez, *Chem. Mater.*, 2009, **291**, 1761.

28 J. Park, K. An, Y. Hwang, J.-G. Park, H.-J. Noh, J.-Y. Kim, J.-H. Park, N.-M. Hwang and T. Hyeon, *Nat. Mater.*, 2004, **3**, 891.

29 S. Sun and H. Zeng, *J. Am. Chem. Soc.*, 2002, 8204.

30 L. Bao, W.-L. Low, J. Jiang and J. Y. Ying, *J. Mater. Chem.*, 2012, **22**, 7117.

31 S. Palchoudhury, W. An, Y. Xu, Y. Qin, Z. Zhang, N. Chopra, R. A. Holler, C. H. Turner and Y. Bao, *Nano Lett.*, 2011, **11**, 1141.

32 N. Du, Y. Xu, H. Zhang, C. Zhai and D. Yang, *Nanoscale Res. Lett.*, 2010, **5**, 1295.

33 Y. C. Zhang, J. Y. Tang and X. Y. Hu, *J. Alloys Compd.*, 2008, **462**, 24.

34 C.-M. Lee, H.-J. Jeong, S. T. Lim, M.-H. Sohn and D. W. Kim, *ACS Appl. Mater. Interfaces*, 2010, **2**, 756.

35 M.-Y. Chang, W.-H. Wang and Y.-C. Chung, *J. Mater. Chem.*, 2011, **21**, 4966.

36 Z. Tang and N. A. Kotov, *Adv. Mater.*, 2005, **17**, 951.

37 S. J. Hurst, E. K. Payne, L. Qin and C. A. Mirkin, *Angew. Chem., Int. Ed.*, 2006, **45**, 2672.

38 J. Yuan, Y. Xu and A. H. E. Müller, *Chem. Soc. Rev.*, 2011, **40**, 640.

39 Y. Liu, J. Goebl and Y. Yin, *Chem. Soc. Rev.*, 2013, **42**, 2610.

40 A. Hultgren, M. Tanase, C. S. Chen, G. J. Meyer and D. H. Reich, *J. Appl. Phys.*, 2003, **93**, 7554.

41 A. Hultgren, M. Tanase, E. J. Felton, K. Bhadriraju, A. K. Salem, C. S. Chen and D. H. Reich, *Biotechnol. Prog.*, 2005, **21**, 509.

42 F. Byrne, A. Prina-Mello, A. Whelan, B. M. Mohamed, A. Davies, Y. K. Gun'ko, J. M. D. Coey and Y. Volkov, *J. Magn. Magn. Mater.*, 2009, **321**, 1341.

43 D. H. Reich, M. Tanase, A. Hultgren, L. A. Bauer, C. S. Chen and G. J. Meyer, *J. Appl. Phys.*, 2003, **93**, 7275.

44 K. B. Lee, S. Park and C. A. Mirkin, *Angew. Chem., Int. Ed.*, 2004, **43**, 3048.

45 B. K. Oh, S. Park, J. E. Millstone, S. W. Lee, K. B. Lee and C. A. Mirkin, *J. Am. Chem. Soc.*, 2006, **128**, 11825.

46 M. Chen, L. Sun, J. E. Bonevich, D. H. Reich, C. L. Chien and P. C. Searson, *Appl. Phys. Lett.*, 2003, **82**, 3310.

47 K. M. Pondman, A. W. Maijenburg, F. B. Celikkol, A. A. Pathan, U. Kishore, B. Ten Haken, J. E. ten Elshof and B. ten Haken, *J. Mater. Chem. B*, 2013, **1**, 6129.

48 J. E. McCarthy, A. Prina-Mello, T. Rakovich, Y. Volkov and Y. K. Gun'ko, *J. Mater. Chem.*, 2011, **21**, 14219.

49 X. Liu, M. D. Kaminski, Y. Guan, H. Chen, H. Liu and A. J. Rosengart, *J. Magn. Magn. Mater.*, 2006, **306**, 248.

50 A. Prina-Mello, A. M. Whelan, A. Atzberger, J. E. McCarthy, F. Byrne, G.-L. Davies, J. M. D. Coey, Y. Volkov and Y. K. Gun'ko, *Small*, 2010, **6**, 247.

51 S. J. Son, J. Reichel, B. He, M. Schuchman and S. B. Lee, *J. Am. Chem. Soc.*, 2005, **127**, 7316.

52 H. H. Yang, S. Q. Zhang, X. L. Chen, Z. X. Zhuang, J. G. Xu and X. R. Wang, *Anal. Chem.*, 2004, **76**, 1316.

53 Z. Liu, D. Zhang, S. Han, C. Li, B. Lei, W. Lu and J. Fang, *J. Am. Chem. Soc.*, 2005, **127**, 6.

54 H. Wu, G. Liu, Y. Zhuang, D. Wu, H. Zhang, H. Yang, H. Hu and S. Yang, *Biomaterials*, 2011, **32**, 4867.

55 Y. J. Lu, K. C. Wei, C. C. M. Ma, S. Y. Yang and J. P. Chen, *Colloids Surf., B*, 2012, **89**, 1.

56 M. Yin, M. Wang, F. Miao, Y. Ji, Z. Tian, H. Shen and N. Jia, *Carbon*, 2012, **50**, 2162.
57 G. Lamanna, A. Garofalo, G. Popa, C. Wilhelm, S. Bégin-Colin, D. Felder-Flesch, A. Bianco, F. Gazeau and C. Ménard-Moyon, *Nanoscale*, 2013, **5**, 4412.
58 A. Demortière, P. Panissod, B. P. Pichon, G. Pourroy, D. Guillon, B. Donnio and S. Bégin-Colin, *Nanoscale*, 2011, **3**, 225.
59 S. J. Byrne, S. A. Corr, Y. K. Gun'ko, J. M. Kelly, D. F. Brougham and S. Ghosh, *Chem. Commun.*, 2004, 2560.
60 H. Jaganathan, R. L. Gieseck and A. Ivanisevic, *J. Phys. Chem. C*, 2010, **114**, 22508.
61 H. Jaganathan, R. L. Gieseck and A. Ivanisevic, *Nanotechnology*, 2010, **21**, 245103.
62 H. Jaganathan, R. L. Gieseck, K. Hudson, M. Kellogg, A. K. Ramaswamy, K. E. Raver, T. Smith, A. N. Vacchiano, A. Wager and A. Ivanisevic, *ChemPhysChem*, 2010, **11**, 3664.
63 H. Jaganathan and A. Ivanisevic, *ACS Appl. Mater. Interfaces*, 2010, **2**, 1407.
64 H. Jaganathan, D. L. Hugar and A. Ivanisevic, *ACS Appl. Mater. Interfaces*, 2011, **3**, 1282.
65 H. Jaganathan and A. Ivanisevic, *J. Mater. Chem.*, 2011, **21**, 939.
66 R. W. Chantrell, A. Bradbury, J. Popplewell and S. W. Charles, *J. Phys. D: Appl. Phys.*, 1980, **13**, L119.
67 M. Klokkenburg, C. Vonk, E. M. Claesson, J. D. Meeldijk, B. H. Erné and A. P. Philipse, *J. Am. Chem. Soc.*, 2004, **126**, 16706.
68 L. Meng, W. Chen, C. Chen, H. Zhou, Q. Peng and Y. Li, *Cryst. Growth Des.*, 2010, **10**, 479.
69 S. Palchoudhury, Y. Xu, J. Goodwin and Y. Bao, *J. Appl. Phys.*, 2011, **109**, 07E314.
70 J. Jia, J. C. Yu, Y.-X. J. Wang and K. M. Chan, *ACS Appl. Mater. Interfaces*, 2010, **2**, 2579.
71 L. He, M. Wang, J. Ge and Y. Yin, *Acc. Chem. Res.*, 2012, **45**, 1431.
72 M. Wang, L. He and Y. Yin, *Mater. Today*, 2013, **16**, 110.
73 R. Sheparovych, Y. Sahoo, M. Motornov, S. Wang, H. Luo, P. N. Prasad, I. Sokolov and S. Minko, *Chem. Mater.*, 2006, 18, 591.
74 J. Fresnais, J.-F. Berret, B. Frka-Petesic, O. Sandre and R. Perzynski, *Adv. Mater.*, 2008, **20**, 3877.
75 J. Fresnais, E. Ishow, O. Sandre and J.-F. Berret, *Small*, 2009, **5**, 2533.
76 M. Safi, M. Yan, M.-A. Guedeau-Boudeville, H. Conjeaud, V. Garnier-Thibaud, N. Boggetto, A. Baeza-Squiban, F. Niedergang, D. Averbeck and J.-F. Berret, *ACS Nano*, 2011, **5**, 5354.
77 D. Fragouli, R. Buonsanti, G. Bertoni, C. Sangregorio, C. Innocenti, A. Falqui, D. Gatteschi, P. D. Cozzoli, A. Athanassiou and R. Cingolani, *ACS Nano*, 2010, **4**, 1873.
78 Y. Sahoo, M. Cheon, S. Wang, H. Luo, E. P. Furlani and P. N. Prasad, *J. Phys. Chem. B*, 2004, **108**, 3380.
79 G. Bertoni, B. Torre, A. Falqui, D. Fragouli, A. Athanassiou and R. Cingolani, *J. Phys. Chem. C*, 2011, **115**, 7249.
80 J. Ge, Y. Hu, M. Biasini, W. P. Beyermann and Y. Yin, *Angew. Chem., Int. Ed.*, 2007, **46**, 4342.
81 Y. Hu, L. He and Y. Yin, *Angew. Chem., Int. Ed.*, 2011, **50**, 3747.
82 H. Wang, Q. W. Chen, L. X. Sun, H. P. Qi, X. Yang, S. Zhou and J. Xiong, *Langmuir*, 2009, **25**, 7135.
83 P. Gambardella, A. Dallmeyer, K. Maiti, M. C. Malagoli, W. Eberhardt, K. Kern and C. Carbone, *Nature*, 2002, **416**, 301.
84 Q. He, T. Yuan, S. Wei, N. Haldolaarachchige, Z. Luo, D. P. Young, A. Khasanov and Z. Guo, *Angew. Chem., Int. Ed.*, 2012, **51**, 8842.
85 Q. He, T. Yuan, X. Yan, Z. Luo, N. Haldolaarachchige, D. P. Young, S. Wei and Z. Guo, *Chem. Commun.*, 2014, **50**, 201.
86 *US Pat.* US5262176, 1993.
87 Q. Liu, S. Shen, Z. Zhou and L. Tian, *Mater. Lett.*, 2009, **63**, 2625–2627.
88 H. Lee, H. S. R. Shin, A. M. Drews, A. M. Chirsan, S. A. Lewis and K. J. M. Bishop, *ACS Nano*, 2014, 9979–9987.
89 P. M. Peiris, E. Schmidt, M. Calabrese and E. Karathanasis, *PLoS One*, 2011, **6**, e15927.
90 P. M. Peiris, L. Bauer, R. Toy, E. Tran, J. Pansky, E. Doolittle, E. Schmidt, E. Hayden, A. Mayer, R. a Keri, M. a Griswold and E. Karathanasis, *ACS Nano*, 2012, **6**, 4157–4168.
91 K. Nakata, Y. Hu, O. Uzun, O. Bakr and F. Stellacci, *Adv. Mater.*, 2008, **20**, 4294.
92 G. A. De Vries, M. Brunnbauer, Y. Hu, A. M. Jackson, B. Long, B. T. Neltner, O. Uzun, B. H. Wunsch and F. Stellacci, *Science*, 2007, **315**, 358.
93 G. A. De Vries, F. R. Talley, R. P. Carney and F. Stellacci, *Adv. Mater.*, 2008, **20**, 4243.
94 A. Verma and F. Stellacci, *Small*, 2010, **6**, 12.
95 F. M. Kievit and M. Zhang, *Acc. Chem. Res.*, 2011, **44**, 853.
96 N. Erathodiyil and J. Y. Ying, *Acc. Chem. Res.*, 2011, **44**, 925.
97 R. Mout, D. F. Moyano, S. Rana and V. M. Rotello, *Chem. Soc. Rev.*, 2012, **41**, 2539.
98 C. D. Walkey and W. C. W. Chan, *Chem. Soc. Rev.*, 2012, **41**, 2780.
99 A. Albanese, P. S. Tang and W. C. W. Chan, *Annu. Rev. Biomed. Eng.*, 2012, **14**, 1.
100 B. Pelaz, G. Charron, C. Pfeiffer, Y. Zhao, J. M. de la Fuente, X.-J. Liang, W. J. Parak and P. Del Pino, *Small*, 2013, **9**, 1573.
101 M. Moros, S. G. Mitchell, V. Grazu and J. M. de la Fuente, *Curr. Med. Chem.*, 2013, **20**, 2759.
102 J.-M. Montenegro, V. Grazu, A. Sukhanova, S. Agarwal, J. M. de la Fuente, I. Nabiev, A. Greiner and W. J. Parak, *Adv. Drug Delivery Rev.*, 2013, **65**, 677.
103 R. M. Fratila, S. G. Mitchell, P. del Pino, V. Grazu and J. M. de la Fuente, *Langmuir*, 2014, 30, 15057

104 M.-M. Song, W.-J. Song, H. Bi, J. Wang, W.-L. Wu, J. Sun and M. Yu, *Biomaterials*, 2010, **31**, 1509.
105 K. Kostarelos, L. Lacerda, G. Pastorin, W. Wu, S. Wieckowski, J. Luangsivilay, S. Godefroy, D. Pantarotto, J.-P. Briand, S. Muller, M. Prato and A. Bianco, *Nat. Nanotechnol.*, 2007, **2**, 108.
106 A. O. Fung, V. Kapadia, E. Pierstorff, D. Ho and Y. Chen, *J. Phys. Chem. C*, 2008, **112**, 15085.
107 K. Donaldson, F. A. Murphy, R. Duffin and C. A. Poland, *Part. Fibre Toxicol.*, 2010, **7**, 5.
108 Y. Liu, Y. Zhao, B. Sun and C. Chen, *Acc. Chem. Res.*, 2013, **46**, 702.
109 P. S. Low and S. A. Kularatne, *Curr. Opin. Chem. Biol.*, 2009, **13**, 256.
110 L. Borlido, A. M. Azevedo, A. C. A. Roque and M. R. Aires-Barros, *Biotechnol. Adv.*, 2013, **31**, 1374.
111 J. Chen, J. Li and Y. Sun, *Lab Chip*, 2012, **12**, 1753.
112 J. He, M. Huang, D. Wang, Z. Zhang and G. Li, *J. Pharm. Biomed. Anal.*, 2014, **101**, 84.
113 C. Kaittanis, S. A. Naser and J. M. Perez, *Nano Lett.*, 2007, **2**, 2.
114 E. Ruoslahti, S. N. Bhatia and M. J. Sailor, *J. Cell Biol.*, 2010, **188**, 759.
115 E. Ruoslahti, *Adv. Mater.*, 2012, **24**, 3747.
116 J. A. Hoffman, E. Giraudo, M. Singh, L. Zhang, M. Inoue, K. Porkka, D. Hanahan and E. Ruoslahti, *Cancer Cell*, 2003, **4**, 383.
117 P. Laakkonen, K. Porkka, J. A. Hoffman and E. Ruoslahti, *Nat. Med.*, 2002, **8**, 751.
118 P. Laakkonen, M. E. Akerman, H. Biliran, M. Yang, F. Ferrer, T. Karpanen, R. M. Hoffman and E. Ruoslahti, *Proc. Natl. Acad. Sci. U. S. A.*, 2004, **101**, 9381.
119 L. Agemy, D. Friedmann-Morvinski, V. R. Kotamraju, L. Roth, K. N. Sugahara, O. M. Girard, R. F. Mattrey, I. M. Verma and E. Ruoslahti, *Proc. Natl. Acad. Sci. U. S. A.*, 2011, **108**, 17450.
120 J.-H. Park, G. von Maltzahn, M. J. Xu, V. Fogal, V. R. Kotamraju, E. Ruoslahti, S. N. Bhatia and M. J. Sailor, *Proc. Natl. Acad. Sci. U. S. A.*, 2010, **107**, 981.
121 G. von Maltzahn, J.-H. Park, K. Y. Lin, N. Singh, C. Schwöppe, R. Mesters, W. E. Berdel, E. Ruoslahti, M. J. Sailor and S. N. Bhatia, *Nat. Mater.*, 2011, **10**, 545.
122 J. H. Lo, G. von Maltzahn, J. Douglass, J.-H. Park, M. J. Sailor, E. Ruoslahti and S. N. Bhatia, *J. Mater. Chem. B*, 2013, **1**, 5235.
123 Y. Matsumoto and A. Jasanoff, *Magn. Reson. Imaging*, 2008, **26**, 994.